A LA-ICP-MS Comparison of Reference Materials Used in Cassiterite U-Pb Geochronology

Patrick Carr, Emeline Moreira, Leonid Neymark, Marc Norman, Julien Mercadier

A LA-ICP-MS comparison of reference materials used in cassiterite U–Pb geochronology

Patrick A. Carr[1*], Emeline Moreira[1], Leonid Neymark[2], Marc D. Norman[3], and Julien Mercadier[1]

[1] Université de Lorraine, CNRS, CREGU, GeoRessources, F-54000 Nancy, France
[2] U.S. Geological Survey, Geology, Geophysics & Geochemistry Science Center, Denver, CO, United States
[3] Research School of Earth Sciences, The Australian National University, Canberra ACT 2601 Australia
* Correspondence: Patrick.carr@univ-lorraine.fr;

Abstract: Laser ablation inductively-coupled mass spectrometry (LA-ICP-MS) is used to compare the suitability of four cassiterites (SPG, Yankee, AY-4, and Jian-1), and three matrix-mismatched reference materials (NIST612, NIST614 and 91500 zircon) for normalisation of U–Pb and Pb-Pb isotope ratios in cassiterite (SnO_2). The excess variance of ages determined by LA-ICP-MS is estimated to be ±0.33% for $^{207}Pb/^{206}Pb$ vs. $^{208}Pb/^{206}Pb$ isochron ages and ±1.8% and for U–Pb ages. Incorporation of this excess variance in cassiterite ages is necessary for realistic uncertainties. ^{207}Pb-^{206}Pb ages are advantageous for dating Precambrian cassiterite such as SPG compared to U–Pb ages as matrix effect on instrumental mass fractionation of Pb isotopes are generally considered to be minor. We note minor bias in $^{207}Pb/^{206}Pb$ vs. $^{208}Pb/^{206}Pb$ isochron ages (*ca* 0.6%) when using either the NIST614 or 91500 zircon reference materials and emphasize the requirement for uncertainty propagation of all sources of error and reference materials with comparable U and Pb mass fraction to the cassiterite. The $^{238}U/^{206}Pb$ isotopic ratios from normalisation to matrix-mismatched reference materials show varied results, which emphasises the need to use matrix-matched reference materials for calculating U–Pb ages. When cross-calibrated against each other, LA-ICP-MS U–Pb ages of the *ca* 1535 Ma SPG, *ca* 245 Ma Yankee, and *ca* 155 Ma Jian-1 cassiterites are all consistent with their ID-TIMS values.

Abstract (Français)

L'ablation laser couplée à la spectrométrie de masse à plasma induit (LA-ICP-MS) est utilisée pour évaluer la validité de quatre cassitérites (SPG, Yankee, AY-4 et Jian-1) et de trois matériaux de référence de matrices différentes (NIST612, NIST614 et zircon 91500) pour la normalisation des rapports isotopiques U–Pb et Pb-Pb dans les cassitérites (SnO_2). La variance de reproductibilité des âges déterminés par LA-ICP-MS est estimée à ±0,33% pour les âges isochrones $^{207}Pb/^{206}Pb$ vs. $^{208}Pb/^{206}Pb$ et ±1,8% pour les âges U-Pb. L'introduction de cette

variance de reproductibilité dans le calcul des âges de cassitérite est nécessaire pour obtenir des incertitudes réalistes. Les âges $^{207}Pb/^{206}Pb$ sont plus favorables que les âges U–Pb pour la datation de cassitérite précambrienne, telle que SPG, puisque l'effet de matrice sur le fractionnement de masse instrumental des isotopes de Pb est généralement considéré comme mineur. Nous constatons un biais mineur dans les âges isochrones $^{207}Pb/^{206}Pb$ vs. $^{208}Pb/^{206}Pb$ (environ 0,6 %), lors de l'utilisation des matériaux de référence NIST614 ou le zircon 91500 et nous soulignons l'importance d'utiliser des matériaux de référence avec des fractions massiques en U et Pb comparable à celle de la cassitérite. Les rapports isotopiques $^{238}U/^{206}Pb$, issus de la normalisation par rapport aux matériaux de référence de matrice différente présentent des résultats variés, ce qui met en évidence la nécessité d'utiliser des matériaux de référence de même matrice pour calculer les âges U–Pb. Lorsqu'ils sont étalonnés les uns par rapport aux autres, les âges U–Pb des cassitérites SPG *ca* 1535 Ma, Yankee *ca* 245 Ma et Jian-1 *ca* 155 Ma, obtenus par LA-ICP-MS, sont en accord avec leurs valeurs obtenues par dilution isotopique et spectrométrie de masse à thermo-ionisation (ID-TIMS).

Keywords: Cassiterite; U–Pb geochronology; LA-ICP-MS

1. Introduction

The U–Pb isotopic composition of cassiterite (SnO_2) has been used to constrain the absolute age and duration of magmatic-hydrothermal Sn(-W) systems (e.g. Gulson and Jones, 1992; Blevin and Norman, 2010; Yuan et al., 2011; Zhang et al., 2017a; Neymark et al., 2018; Cheng et al., 2019; Rizvanova and Kuznetsov, 2020; Carr et al., 2020; Tapster and Bright, 2020; Denholm et al., 2021; Gemmrich et al., 2021; Marcoux et al., 2021) and rare-metal pegmatite systems (Kendall-Langley et al., 2020; Liu et al., 2020a; Nambaje et al., 2021). The advantages of using cassiterite instead of other geochronometers within these deposits is that cassiterite directly dates the Sn mineralising event rather than relying on minerals assumed to be cogenetic with the alteration (e.g., Rb-Sr dating of micas). Additionally, cassiterite is resistant to chemical and physical abrasion such that it can preserve its primary U–Pb isotopic composition through pervasive hydrothermal alteration (e.g., Carr et al., 2020), passage through the sedimentary cycle (e.g., Oberthür et al., 2016) and even magmatic recycling as evidenced from age inheritance identified within cassiterite grains (Neymark et al., 2021a).

Recent advances in the chemical decomposition of cassiterite using HBr acid dissolution techniques (Carr et al., 2020; Tapster and Bright, 2020; Yang et al. 2022) now permit high precision determination of U–Pb and Pb-Pb isotopic compositions by isotope dilution thermal ionisation mass spectrometry (ID-TIMS). These new methods can determine U–Pb isotopic ratios of cassiterite with a precision better than 0.1% and provide exciting new high-resolution constraints on the temporal evolution of the magmatic-hydrothermal systems that produce tin mineralisation (Tapster and Bright, 2020). However, the robust chemical stability of cassiterite prior to ID-TIMS analyses requires long sample processing times (e.g., ~5 days for dissolution; Tapster and Bright, 2020), which restricts the applicability of this technique to a small number of samples. Therefore, *in situ* techniques like laser ablation inductively-coupled mass spectrometry (LA-ICP-MS) have recently been the most popular method for U–Pb cassiterite geochronology due to rapid data generation and limited sample preparation (e.g., Li et al., 2016; Oberthür et al., 2016; Zhang et al., 2017a; Neymark et al., 2018, 2021a and b; Cheng et al., 2019; Kendall-Langley et al., 2020; Moscati and Neymark, 2020; Liu et al., 2020b; Denholm et al., 2021). Note that LA-ICP-MS refers to a group of instrumental setups with different mass analysers (e.g., quadrupole (Q) or sector-field (SF)) and ion-counting (single collector (SC) or multi-collector (MC)) techniques, but for this paper we use the general term unless specified otherwise.

U–Pb ages determined by LA-ICP-MS are inherently less precise relative to ID-TIMS ages due to the relatively small amount of material ablated per analysis that yields transient and generally low signals on the measured isotopes. In addition, U–Pb isotope ratios (i.e., $^{206}Pb/^{238}U$ and $^{207}Pb/^{235}U$) measured by LA-ICP-MS in a variety of mineral matrices require large corrections to account for laser-induced elemental fractionation (LIEF) and instrumental mass fractionation (IMF; mass-dependent bias of the measured isotope ratios from those in the sample). The mechanisms of elemental and isotope fractionation by LIEF and IMF during LA- and ICP-MS, respectively, are broadly understood (e.g., Guillong et al., 2003; Yu et al., 2003; Kroslakova and Günther, 2007a; Kuhn et al., 2010a; Fietzke and Frische, 2016), however, correction for their combined effects is made empirically using matrix-matched reference materials with a well-defined U–Pb age and common Pb composition that is analysed throughout an analytical session (e.g., Jackson et al., 2004). In the absence of cassiterite reference materials with high precision ID-TIMS U–Pb data, Neymark et al. (2018) presented a new method of normalisation of LA-ICP-MS data. In this method, the true $^{238}U/^{206}Pb^*$ (where Pb* represents radiogenic Pb) is calculated from a $^{208}Pb/^{206}Pb$ vs. ^{207}Pb-^{206}Pb isochron age determined in a Precambrian cassiterite reference material, assuming all ^{208}Pb is non-radiogenic and concordance between $^{207}Pb/^{235}U$ and $^{206}Pb/^{238}U$ ages. The quotient of this $^{238}U/^{206}Pb^*$ ratio and the measured $^{238}U/^{206}Pb^*$ ratio (determined from a lower intercept biased age on a $^{238}U/^{206}Pb$ vs. ^{207}Pb-

^{206}Pb diagram) provides a matrix-matched session correction factor. This method benefits from the fact that Pb-Pb ages of Precambrian cassiterite are more easily obtained by LA-ICP-MS compared to the U–Pb age because IMF effects on Pb isotopes are often considered insignificant relative to the total uncertainty of LA-ICP-MS analyses, and Pb isotope ratios can be normalised to non-matrix matched references materials such as the NIST synthetic glasses (e.g., Pietruszka and Neymark, 2017).

A few studies have proposed the use of matrix-mismatched reference materials for normalisation of U–Pb ratios in cassiterite including the NIST612 glass (Cheng et al., 2019; Kendall-Langley et al., 2020), zircon (Yuan et al., 2011; Oberthür et al., 2016), baddeleyite (Marcoux et al., 2021) and rutile (Gemmrich et al., 2021). These studies and others have noted significant bias in U–Pb cassiterite ages determined by LA-ICP-MS systems when using a NIST612 (up to 15%) (Blevin and Norman, 2010a; Neymark et al., 2018), zircon (*ca* 7%) (Neymark et al., 2018), and rutile (*ca* 8%) as the primary reference material and have suggested that this approach is inaccurate and not reproducible. Note that the relative offset of U–Pb ages from these matrix-mismatched studies is dependent on the laser spot properties used.

The uncertainty of U–Pb ages determined by LA-ICP-MS must encompass the intra- (instrument drift) and inter- session (i.e., excess variance; ε') reproducibility which typically is quantified by repeated analyses of primary and secondary reference materials, respectively. In the zircon U-Pb geochronology literature, the excess variance for LA-ICP-MS is estimated at *ca* 1.5% (Horstwood et al., 2016), and this represents a minimum age uncertainty obtainable by this method. Currently, very few reference cassiterites with well-defined U–Pb ages and common Pb composition exist to quantify intra- and inter- session reproducibility. This is largely due to the time-consuming process of obtaining high precision ID-TIMS data. For this reason, many studies report only the repeatability (i.e., 'in-run') precision of better than 1.5% for individual analytical sessions which is likely unrealistically small . Therefore, the use of multiple cassiterite reference materials in an analytical session for normalisation and validation of U–Pb data (Liu et al., 2021) will yield more robust ages and realistic uncertainties of U–Pb cassiterite ages, as currently applied for *in situ* zircon geochronology (e.g., Horstwood et al. 2016).

For this study, we analysed four cassiterites previously analysed by ID-TIMS and that have been used as U–Pb reference materials for LA-ICP-MS analyses (SPG, Yankee, AY-4, and Jian-1). Additionally, we include the 91500 zircon, NIST612 and NIST614 matrix-mismatched materials to assess their suitability for use as reference materials of U–Pb and Pb-Pb cassiterite ages determined by LA-ICP-MS. Using these materials, we quantify reasonable uncertainties for U–Pb and Pb-Pb ages and compare the traditional data

reduction methods (e.g., Paton et al., 2011; Chew et al., 2014) using both matrix-matched and -mismatched materials with the novel approach described in Neymark et al. (2018). Finally, we summarise the important characteristics of each of the studied cassiterite, including its availability to laboratories, internal chemical and petrographic features.

2. Materials

The first ID-TIMS study of cassiterite yielded variable results probably due to the incomplete digestion of cassiterite in HCl prior to analysis (Gulson and Jones, 1992) and subsequently no cassiterites from that study have been used as reference materials. The vast majority of published LA-ICP-MS studies have used the AY-4 cassiterite from the Furong deposit in the Nanling Range, Hunan Province, P.R. China, following the initial publication of ID-TIMS data by Yuan et al., (2011) and subsequently by Carr et al. (2020) and Yang et al. (2022). More recently, three ID-TIMS studies based on HBr digestion have presented U–Pb compositions of the Yankee cassiterite from eastern Australia (Carr et al., 2020), the SPG from the Russian Karelia (Tapster and Bright, 2020), Jian-1 from the Nanling Range (Tapster and Bright, 2020), and cassiterite from Cligga Head of the Cornubian Batholith, SW England (Tapster and Bright, 2020). Note that the U–Pb isotopic compositions of SPG and Jian-1 were originally characterised by LA-ICP-MS in Neymark et al. (2018). In Figure 1 we present a summary of published U–Pb ages of the cassiterite used in this study. In addition, we use three matrix-mismatched materials including the 91500 zircon (Wiedenbeck et al., 1995) and the NIST612 and NIST614 synthetic glasses (U–Pb data found in Baker et al., 2004) to test their suitability for U–Pb cassiterite geochronology.

2.1. Pitkäranta ore district, Russian Karelia (SPG)

Cassiterite of the Pitkäranta ore district in the Russian Karelia (Larin et al., 1991 and references therein) occurs in skarn deposits. Skarn mineralisation is associated with late intrusions within the 1.55–1.53 Ga Salmi anorthosite rapakivi granite batholith (Amelin et al., 1991, 1997; Larin et al., 1991; Neymark et al., 1994) and U–Pb ages of zircons from this batholith range from 1547 Ma to 1530 Ma (Amelin et al., 1997). Multi-mineral and whole rock Sm-Nd isochron ages of the skarn and an associated greisen deposit are 1546 ± 20 Ma and 1491 ± 42 Ma, respectively (Amelin et al., 1991). *In situ* LA-ICP-MS U–Pb and Pb-Pb ages for six cassiterite samples from the skarns range from 1536 ± 25 Ma to 1551 ± 28 Ma (Neymark et al., 2021b).

Samples SPG-II and SPG-IV (aliquots of sample SPG) were collected from a pyroxene-garnet skarn. As both the SPG-II and -IV aliquots have similar U–Pb ages, we refer only to the sample name SPG for simplicity. Tapster

and Bright (2020) present U–Pb isotopic compositions of the SPG determined by ID-TIMS. The three aliquots were slightly discordant due to common Pb, and the authors present two lower intercept ages of 1535.9 ± 5.5 Ma when the regression is unconstrained and 1536.6 ± 1.0 Ma when initial $^{207}Pb/^{206}Pb_i$ is anchored to 1.0104 ± 0.0062 (determined on galena from the same deposit; Larin et al., 1991) and a $^{204}Pb/^{206}Pb$ vs. $^{207}Pb/^{206}Pb$ isochron age of 1540.9 ± 3.6 Ma. A different ID-TIMS study found a U–Pb Concordia intercept age of 1539.53 ± 0.90 Ma from two aliquots of the SPG (Rizvanova and Kuznetsov, 2020). The weighted mean $^{207}Pb/^{206}Pb$ age of these two aliquots is 1539.55 ± 0.46 Ma. Neymark et al. (2018) report a LA-ICP-MS $^{207}Pb/^{206}Pb$ age of 1542.7 ± 1.5 Ma (2SE, 2 standard error) after normalisation of Pb isotopic ratios to the NIST612 glass.

2.2. Yankee deposit, Australia

The Yankee Sn deposit is one of over 1200 polymetallic deposits occurring within and adjacent to the highly fractionated Mole Granite of eastern Australia (Brown and Stroud, 1997). The deposit includes quartz-cassiterite veins that are 10 to 40 cm thick. Initially, cassiterite was obtained from the state collection of the Geological Survey of NSW and contained cassiterite grains of 0.4–1 mm in diameter occurring in large vugs within ore veins (Blevin and Norman, 2010a; Carr et al., 2017, 2020). A detailed description of the Yankee deposit is available in Brown and Stroud (1997; pg. 55).

The Yankee cassiterite has an ID-TIMS 'Total-Pb/U isochron' intercept age of 246.48 ± 0.51/0.55/0.62 Ma (where the uncertainties are added sequentially in quadrature and are defined as age/with tracer uncertainty/with decay constant uncertainty) (Carr et al., 2020). The cassiterite age is within uncertainty of a U–Pb age of 246.2 ± 0.5 Ma for hydrothermal xenotime within cassiterite-bearing veins in the Yankee deposit and slightly younger than a U–Pb age of 247.7 ± 0.5 Ma for magmatic zircon and monazite of the Mole Granite (Schaltegger et al., 2005). Since the initial analyses presented in Carr et al. (2020), a new batch of somewhat larger (~1 cm) cassiterite grains was received from the state collection of the Geological Survey of NSW; aliquots of these grains have been distributed to interested laboratories and are used here. Yang et al. (2022) present a LA-SF-ICP-MS $^{238}U/^{206}Pb$ vs $^{207}Pb/^{206}Pb$ lower intercept age of 246.4 ± 2.9 Ma after normalisation of measured values to the SPG cassiterite.

2.3. Nanling Range, South China (AY-4 and Jian-1)

2.3.1. AY-4

The AY-4 cassiterite is from the Bailashui–Anyuan ore belt within Furong deposit of the Hunan Province, China. Mineralisation is within skarn at the contact between Permian carbonate rocks and granite (Yuan et al.,

2011). The granite is associated with the Qitanling granite batholith, which has zircon U–Pb ages that indicate three stages of emplacement between 163–160 Ma, 157–153 Ma and 150–146 Ma (Jingwen et al., 2010). Multiple ^{39}Ar-^{40}Ar ages from muscovite, hornblende, and phlogopite associated with greisenisation within the Furong deposit fall between 160 and 150 Ma (Peng et al., 2007; Jingwen et al., 2010).

The first U–Pb isotopic study of the AY-4 cassiterite reported a U–Pb ID-TIMS age of 158.2 ± 0.4 Ma based on 3 aliquots of the cassiterite digested in HCl (Yuan et al., 2011). Subsequently, two younger ID-TIMS U–Pb ages of 151.9 ± 2.2 Ma (n=3; Carr etal. 2020) and 154.3 ± 0.7 Ma (n= 6; Yang et al. 2022) were reported after HBr dissolution. Since the initial publication, many studies have used the AY-4 as the primary matrix-matched reference material for *in situ* LA-ICP-MS cassiterite U–Pb geochronology and assumed its age of 158.2 ± 0.4 Ma (e.g., Li et al., 2016; Cao et al., 2017; Zhang et al., 2017a, 2019; Guo et al., 2018; Deng et al., 2018; Yang et al., 2020; Fei et al., 2020).

2.3.2. Jian-1

Cassiterite Jian-1 was purchased at a mineral show in Denver, USA, in 2017 and was said to originate from Chongyi, Jiangxi, China. No other location information is available for this sample. The Jiangxi W-Sn district has a multistage magmatic emplacement history between 170 and 150 Ma (Chengyou et al., 2012). Cassiterite mineralisation in this region occurs in quartz veins, greisen and skarn deposits associated with granitic rocks (Chengyou et al., 2012). A LA-ICP-MS age of 156.6 ± 0.4 Ma (only session reproducibility reported) was determined after normalisation to the SPG cassiterite (Neymark et al., 2018). Subsequently this age has been superseded by a lower intercept age of 154.97 ± 0.08 Ma based on ID-TIMS data obtained on four aliquots (Tapster and Bright, 2020).

3. Methods

3.1. Sample preparation and cathodoluminescence (CL) imaging of cassiterite

Handpicked cassiterite grains were placed onto double-sided tape under a binocular microscope, mounted in epoxy, ground to expose the grain interior using 1500-grit sandpaper, and polished sequentially using 6 µm and 1 µm diamond suspension pastes. Prior to *in situ* analysis, all samples were imaged in transmitted and/or reflected light on a petrographic microscope, and examined for compositional zoning and the presence of inclusions using back-scattered electron (BSE) and CL images from the scanning electron microscopes JEOL 5800LV™ and FEI

Quanta 450 FEG™ operated at 10 keV, beam intensity of 18 nA and 20-mm working distance with a photomultiplier tube at the United States Geological Survey (USGS) Microbeam Laboratory in Denver, Colorado, USA and a TESCAN VEGA3 LM conventional scanning electron microscope (SEM) equipped with a Gatan ChromaCL2UV CL detector at GeoRessources, Université de Lorraine and an operating voltage of 25 keV, beam intensity of 18 nA and working distance of 15 mm.

3.2. U–Pb isotopes by LA-SF-ICP-MS

U–Pb isotopic compositions of all materials were measured in two laboratories at GeoRessources, Université de Lorraine, France, and at USGS, Denver, USA. Key technical parameters used in each laboratory are summarised below and included in Table 1.

3.2.1. GeoRessources, Université de Lorraine, France

U–Pb compositions of all materials were analysed at GeoRessources on a Nu Instruments AttoM^{TM} ES sector field inductively-coupled mass spectrometer (SF-ICP-MS) coupled to an ESI 193 nm, ArF excimer laser ablation system with a two-volume 'TwoVol2' sample cell. Gas flow rates and ion lens parameters were optimised on the NIST 612 glass in line scan mode to provide the highest sensitivity of the measured isotopes whilst maintaining low oxide levels (ThO/Th < 0.05%) and to minimize the fractionation of Th/U, which was typically from 0.93 to 0.97 for NIST612 (accepted value = 1.01; Jochum et al., 2011). Maximum gas blank signal intensities were 180 counts per second (cps) for ^{206}Pb, 140 cps for ^{207}Pb, 330 cps for ^{208}Pb, 2 cps for ^{232}Th, and 100 cps for ^{238}U. The measurement of U (^{238}U and ^{235}U), Th (^{232}Th), and Pb (^{204}Pb, ^{206}Pb, ^{207}Pb and ^{208}Pb) isotopes was conducted using fast-scanning ion deflectors to place a series of flat-topped isotope peaks into a single ion-counting detector. Deflection of the ion beam is performed at a fixed accelerating voltage (~6000 V) and magnetic field strength.

Each sample consisted of multiple grains that were analysed during at least three analytical sessions. Three analytical sessions were carried out in a 'round-robin' style comparison of the four cassiterite studied here. During these sessions and under the same analytical conditions, we also analysed the 91500 zircon (Wiedenbeck et al., 1995) and NIST614 (Baker et al., 2004) to test their applicability to cassiterite U–Pb geochronology. Additional sessions were carried out during 2021 and 2022 using only the Yankee and Jian-1 cassiterite. Prior to each analysis the targeted region was ablated with 5 pulses of a larger and lower-energy dense (2 J/cm^2) laser spot to remove surficial Pb. The analytical approaches to calibration and correction for LIEF and IMF are described in section 3.2.3.

3.2.2. USGS, Denver, USA

U–Pb isotopic compositions of all materials were analysed at USGS following procedures described previously (Neymark et al., 2018). All data were collected during multiple sessions between 2017 and 2019 with laser spot diameters of 85–135 µm, a laser repetition rate of 5 Hz and laser energy density of between 4.0 and 5.0 J/cm^2. The U–Pb data for SPG- and Jian-1 were presented initially in Neymark et al. (2018) and are also discussed here. Data from 5 new analytical sessions including the Jian-1, SPG samples have been added to Appendix A. The U–Pb data from the Yankee and AY-4 are presented here for the first time. Typical gas blank signal intensities were 90-120 cps for ^{206}Pb, 80-110 cps for ^{207}Pb, 200-250 cps for ^{208}Pb, 1-2 cps for ^{232}Th, and 70-100 cps for ^{238}U.

3.2.3. Normalisation of Pb-Pb and U–Pb ratios

Measured U–Pb and Pb-Pb isotope ratios were corrected for LIEF and IMF by two different methods employed by GeoRessources and USGS, separately. All isotope ratio uncertainties are reported at the 2SE (2 × standard error where SE=SD/$\sqrt{n}$, where SD is the sample standard deviation and n is the number of values) level and ages at the 95% confidence level with overdispersion (= 95% conf. int. × √MSWD; Mean Square of Weighted Deviates).

At GeoRessources, measured U–Pb isotopic compositions were reduced in Iolite™ 4 using the UComPbine data reduction scheme (DRS; Paton et al., 2011). We normalise ^{207}Pb/^{206}Pb and ^{208}Pb/^{206}Pb compositions to two reference materials for comparison: the NIST614 glass with accepted values of ^{207}Pb/^{206}Pb = 0.87101 ± 0.00042 and ^{208}Pb/^{206}Pb = 2.1017 ± 0.0007 (Baker et al., 2004) and the 91500 zircon with accepted values of ^{207}Pb/^{206}Pb = 0.07488 ± 0.00001 and ^{208}Pb/^{206}Pb = 0.10690 ± 0.00051 (Wiedenbeck et al., 1995). When counts per second on ^{238}U exceeds 2.0 × 10^6 the ^{238}U/^{206}Pb ratios are calculated from ^{235}U and assuming a ^{238}U/^{235}U of 137.818 (Heiss et al. 2012). This ensures that U isotopes are measured in non-attenuated mode and avoids additional errors associated with uncertainties in attenuation factors. This correction is applied point-by-point in the UComPbine data reduction scheme (DRS; Paton et al., 2011). Note, however, that this assumes negligible IMF between the U isotopes. ^{238}U/^{206}Pb ratios were normalised to four cassiterite reference materials: the Yankee cassiterite assuming ^{238}U/^{206}Pb*=25.66 ± 0.05 corresponding to an age of 246.48 ± 0.51 Ma (Carr et al., 2020), the SPG with ^{238}U/^{206}Pb* =3.717 ± 0.002 corresponding to an age of 1536.6 ± 1.0 Ma (Tapster and Bright, 2020), the AY-4 with ^{238}U/^{206}Pb* =41.28 ± 0.17 corresponding to an age of 154.3 ± 0.8 Ma (Yang et al., 2022), and the Jian-1 cassiterite assuming an ideal composition of ^{238}U/^{206}Pb* = 41.10 ± 0.02 corresponding to an age of 154.94 ± 0.08 Ma (Tapster and Bright, 2020). In the DRS used, the ^{238}U/^{206}Pb of the primary cassiterite reference materials is corrected initially

for common Pb prior to normalisation by assuming an initial $^{207}Pb/^{206}Pb$ of 0.74 ± 0.10 for the Yankee cassiterite (Carr et al., 2020), 1.0104 ± 0.0062 for the SPG (Tapster and Bright, 2020) and 0.85 ± 0.01 for the AY-4 and Jian-1 cassiterites (Stacey and Kramers, 1975). Isochron ages were calculated using the online IsoplotR program (Vermeesch, 2018).

The measured U–Pb and Pb-Pb ratios of USGS were initially corrected using the U_Pb_Geochronology3 DRS of Iolite™ (Paton et al., 2011) using the NIST612 glass as the primary reference material. The assumed $^{207}Pb/^{206}Pb$ and $^{208}Pb/^{206}Pb$ compositions of NIST612 were 0.90745 ± 0.0004 and 2.1651 ± 0.0001, respectively (Baker et al., 2004). The assumed $^{238}U/^{206}Pb$ of NIST612 was 3.456 ± 0.019 that was calculated from the published concentration data (Jochum et al., 2011). NIST-normalised Pb-isotope ratios calculated by Iolite™ were then used for further data reduction and age calculations. Using the Pb-Pb age of the SPG cassiterite, we calculate an ideal $^{238}U/^{206}Pb$ of the cassiterite that would correspond the Pb-Pb age, with the quotient of the NIST612-corrected $^{238}U/^{206}Pb$ and the $^{238}U/^{206}Pb$ calculated from the Pb-Pb age providing a correction factor for the analytical session. Note that new ID-TIMS data of SPG (Tapster and Bright, 2020) yield a younger age than the Pb-Pb age determined by LA-ICP-MS, however, we use the latter in order to test the accuracy of this method without the insight of ID-TIMS data.

Ages were calculated using Isoplot v. 4.15 (Ludwig, 2008). We determine $^{207}Pb/^{206}Pb$–$^{208}Pb/^{206}Pb$ isochrons ages that are analogous to inverse $^{207}Pb/^{206}Pb$–$^{204}Pb/^{206}Pb$ isochrons (Ludwig, 2008) commonly applied to chondritic meteorites. The generally low Th contents of cassiterite indicate negligible *in situ* produced radiogenic ^{208}Pb (Neymark et al., 2018) and a good estimation of common Pb. In the isochron diagrams the age is determined from the y-intercept of the isochron that yields the radiogenic $^{207}Pb^*/^{206}Pb^*$ of the sample.

Excess uncertainty of $^{207}Pb/^{206}Pb$–$^{208}Pb/^{206}Pb$ isochrons ages and $^{207}Pb/^{206}Pb$ vs $^{238}U/^{206}Pb$ lower intercept ages are estimated in section 4.4. Ages and their uncertainties are reported in the format a ± b (c) Ma where a is the age in millions of years before the present, b is the within-session reproducibility and c is the total uncertainty that includes b, decay constant uncertainty and the excess variation added in quadrature.

3.2.4. Pb, Th and U mass fraction

Total Pb, Th and U mass fractions in the cassiterite were estimated by normalising the raw measured count rates in cps of each isotope to that measured in the NIST614 glass (accepted values: Pb = 2.32 µg/g, Th = 0.748 µg/g and U = 0.823 µg/g; Jochum et al., 2011) at GeoRessources and NIST612 glass (accepted values: Pb = 38.57 µg/g, Th = 37.79 µg/g and U = 37.38 µg/g; Jochum et al., 2011) at USGS. To account for the difference in Pb

isotopic composition between NIST glasses and cassiterite, the measured intensities for ^{206}Pb, ^{207}Pb and ^{208}Pb were summed to give a 'total Pb' intensity. The two AttoM ES ICP-MS instruments used fast-scanning ion deflectors to sequentially place isotope peaks into a single ion-counting detector and in this mode have a limited mass range (~40%) so an internal standard element (i.e., Sn) could not be included in the mass sweep. Due to the significantly different matrices between cassiterite and the NIST glasses we assume an uncertainty of 20% on element mass fractions (Neymark et al., 2018).

4. Results

4.1 Crystallographic features of cassiterite

Cathodoluminescence images of cassiterite are shown in Figures 2 (SPG and Yankee) and 3 (AY-4 and Jian-1). The grain size (75–200 µm) and rare secondary alteration of the SPG cassiterite allows for laser spot diameters of frequently >90 µm. This cassiterite is generally featureless in CL images (Figure 2A), however, concentric zoning is evident in some grains.

The Yankee deposit cassiterite can vary from 'gem-quality' euhedral crystals with resinous lustre, and no apparent alteration, to subhedral crystals with visible alteration and intergrown quartz. Gem-quality Yankee cassiterite is dominated by primary growth features such as concentric and sector zoning that are defined in the CL images (Figure 2B). Internal zones within the cassiterite that display a quenched afterglow (i.e., dark CL response) are notably more enriched in U and are therefore favourable for U–Pb analyses (Carr et al., 2017). Other, less pristine crystals have secondary features such as the resorption of primary textures (Figure 2B) and internal cracks with alteration selvage.

AY-4 grains used in this study measure between 100 and 500 µm. Cathodoluminescence imaging shows common oscillatory zoning within grains that define both diffuse and abrupt terminations prior to the adjacent lamination (Figure 3A). Resorption of primary textures can occur (e.g., Figure 3A). Mineral inclusions are common, and during this study unstable signals on all measured isotopes were observed due to ablation of these inclusions that were hidden at the surface. Only the portions of the signal that were not clearly contaminated by these inclusions were selected.

Jian-1 crystal fragments that have been analysed are >500 µm, permitting large laser spot diameters if necessary. Oscillatory zoning, shown in CL images of Figure 3B, is the dominant textural characteristic of the Jian-1 cassiterite. Alteration features and mineral inclusions are rare although an internal network of cracks with a bright CL response is present.

4.2 Pb, Th and U mass fraction

Box and whisker plots of the U mass fraction (in µg/g) and the proportion of common/or initial ^{206}Pb ($^{206}Pb_c$) relative to total Pb ($^{206}Pb_t$) and expressed as f206c are shown in Figures 4A and 4B, respectively.

f206c is calculated according to the following equation (Williams, 1998):

$$f206c=({}_7R_m-{}_7R_*)/({}_7R_c-{}_7R_*)$$

where ${}_7R_m$ is the measured $^{207}Pb/^{206}Pb$, ${}_7R_*$ is the radiogenic $^{207}Pb/^{206}Pb$ (determined iteratively), and ${}_7R_c$ is the non-radiogenic $^{207}Pb/^{206}Pb$. We estimate the ${}_7R_c$ using the values described in section 3.2.3.

SPG has on average the highest U contents of the cassiterites studied here with a mass fraction that varies between 2.2 and 250 µg/g (Figure 4A). Analyses of the SPG generally contain little common Pb and 194 of 227 analyses have a f206c <0.05. The U mass fraction within the Yankee cassiterite is relatively restricted between 4.2–52 µg/g, and generally contains little common Pb (129 of 162 analyses with f206c <0.05). Gem quality crystals have lower U µg/g and f206c compared to altered crystals. The AY-4 cassiterite is highly variable in U (8.6–317 µg/g) which is a much greater range than apparent in the ID-TIMS data (Figure 4). f206c is highly variable with 77 of 139 analyses <0.05, however, this is generally lower than the range observed in ID-TIMS data. The U mass fraction in Jian-1 is variable between 0.86 and 52 µg/g. Analyses of Jian-1 generally have little common Pb with 257 of 281 having f206c <0.05.

4.3 Excess variance of Pb-Pb and U–Pb cassiterite ages

Repeated analyses of reference materials using different laboratories, analytical set-ups and data treatment methods allows for the determination of excess variation of Pb-Pb and U–Pb cassiterite ages. For $^{208}Pb/^{206}Pb$–^{207}Pb-^{206}Pb isochron ages, only the SPG has been analysed enough times at both laboratories to determine an excess variance ±0.33% (Figure 5A). For U–Pb ages, only the Jian-1 has been analysed enough times at both laboratories to determine an excess variance ±1.9% (Figure 5B). Excess variance of U–Pb ages of all cassiterite and normalisation methods relative to the accepted values is ±1.8% (Figure 5C).

4.4 Pb-Pb and U–Pb ages of cassiterite

Pb-Pb and U–Pb isotopic compositions and ages using matrix-matched and mismatched reference materials are listed in Appendices A–D.

4.4.1 $^{208}Pb/^{206}Pb$–^{207}Pb-^{206}Pb isochron ages

$^{208}Pb/^{206}Pb$–^{207}Pb-^{206}Pb isochron ages of SPG vary between *ca* 1535.7 ± 9.9 (11.1) Ma and 1542.6 ± 17.3 (18.1) Ma when normalised to the NIST614 or the NIST612, with a mean age of 1539.7 ± 6.1 (8.0) Ma for all analytical sessions (n=8). In contrast, $^{208}Pb/^{206}Pb$–^{207}Pb-^{206}Pb isochron ages of between 1527.1 ± 6.9 (8.6) Ma and 1533.8 ± 5.8 (7.6) Ma were obtained when normalised to the 91500 zircon with a mean age of 1531.1 ± 7.1 (8.68) Ma for the three analytical sessions where the zircon was included. A comparison of $^{208}Pb/^{206}Pb$–^{207}Pb-^{206}Pb isochron ages from a single session but normalised to the NIST614 and 91500 zircon is shown in Figure 6. Both methods yield ages within uncertainty of the ID-TIMS determined age of 1536.6 ± 1.0 Ma. $^{208}Pb/^{206}Pb$–$^{207}Pb/^{206}Pb$ isochron ages for the Yankee, AY-4, and Jian-1 cassiterites have high uncertainty for individual sessions (> *ca* 10%) and inter-session variability (30%) that suggest this method is not appropriate for samples of this geologically young age.

4.4.2 U–Pb ages

We note very minor difference in lower intercept ages on $^{207}Pb/^{206}Pb$ vs. $^{238}U/^{206}Pb$ diagrams using Pb-Pb data normalised to either the NIST614 or 91500 zircon, therefore in the following sections we discuss only lower intercept ages determined from NIST614 or NIST612 normalised Pb-Pb data.

Average U–Pb ages of cassiterite obtained using matrix-matched reference materials are within uncertainty of the accepted ages for those samples (Figure 5C). It is noteworthy that for numerous sessions, the determined ages without consideration of excess variance are biased from the accepted ages. The within-session uncertainty of ages varied between 0.24 and 3.5%, whereas the inter-session 2SD reproducibility of ages varied between 0.5 and 3.4%.

U–Pb ages of cassiterite using matrix mis-matched reference materials were highly variable between sessions and material used (Figure 7). In general, ages normalised to the NIST614 underestimated the assumed age for each sample by up to 8.5%. Ages normalised to the 91500 zircon are within -2.5% of the assumed age for the first two analytical sessions at GeoRessources but overestimate the age by up to 9.4 % for the third analytical session.

5. Discussion

5.1. Geochronology of 'old' cassiterite

Spencer et al. (2016) showed that $^{207}Pb/^{206}Pb$ ages measured by LA-ICP-MS are generally more precise than U–Pb ages for zircon older than *ca* 1.5 Ga because measured $^{207}Pb/^{206}Pb$ ratios require only minor corrections

for IMF compared to LIEF-corrected $^{238}U/^{206}Pb$, and the older minerals have sufficient radiogenic ^{207}Pb to yield well-defined $^{207}Pb/^{206}Pb$ ages. Cassiterite often contains some common Pb so $^{207}Pb/^{206}Pb$ ages must be determined using a $^{208}Pb/^{206}Pb$–$^{207}Pb/^{206}Pb$ isochron as the ^{208}Pb can be considered entirely non-radiogenic in low-Th cassiterite (Neymark et al., 2018). Excess variance of $^{208}Pb/^{206}Pb$–$^{207}Pb/^{206}Pb$ isochron ages for LA-ICP-MS systems is estimated here at *ca* 0.33% and the total uncertainty of $^{208}Pb/^{206}Pb$–$^{207}Pb/^{206}Pb$ isochron ages is dominantly controlled by the measurement uncertainty and natural heterogeneity (session age uncertainties are typically in the range of 0.36 and 1.2%).

The mean $^{208}Pb/^{206}Pb$–$^{207}Pb/^{206}Pb$ isochron age of the SPG for all data presented in Neymark et al. (2018) and here is 1540.9 ± 12.0 (13.1) Ma (2SD; n=43), within uncertainty of the ID-TIMS U–Pb ages of 1536 ± 1.0 Ma (Tapster and Bright, 2020) and 1539.53 ± 0.90 Ma (Rizvanova and Kuznetsov, 2020). We note that the original age of the SPG published in Neymark et al. (2018) of 1542.7 ± 1.5 (2SE) Ma was older than the subsequent U–Pb ID-TIMS U–Pb age (this did not include excess variance) and emphasise that 2SD is a better estimate of the true uncertainty than the 2SE. $^{208}Pb/^{206}Pb$–$^{207}Pb/^{206}Pb$ isochron ages determined in cassiterite using methods similar to Neymark et al. (2018) and without high precision ID-TIMS age data (Kendall-Langley et al., 2020; Denholm et al., 2021) therefore require multiple analytical sessions to determine the 2SD uncertainty in the age of the reference material in addition to the propagation of excess variance uncertainty.

5.1.1. Pb-Pb normalisation of cassiterite

The individual session $^{208}Pb/^{206}Pb$–$^{207}Pb/^{206}Pb$ isochron ages reported here agree with the published ID-TIMS ages of the SPG (Appendix D). Despite these apparently accurate ages, a difference of between 0.5 and 0.8% is observed in ages between 91500 zircon and NIST614 normalised Pb-Pb ratios using the same dataset and indicates that some matrix-mismatched reference materials can introduce bias. $^{208}Pb/^{206}Pb$–$^{207}Pb/^{206}Pb$ isochron ages determined from data normalised to the 91500 zircon slightly underestimate the age of the SPG (or lower corrected $^{207}Pb^*/^{206}Pb^*$), whilst those ages normalised to the NIST614 are slightly overestimated, although within uncertainty of its accepted age (or higher corrected $^{207}Pb^*/^{206}Pb^*$).

A minor systematic bias towards heavier isotopes is clearly observed in all analysed materials in the measured data, and the magnitude of this bias is different between materials. For example, within a single session the measured $^{207}Pb/^{206}Pb$ and $^{208}Pb/^{206}Pb$ are 0.4% and 1% higher, respectively, in the NIST614 than the accepted values, and 0.8% and 3.2% higher, respectively, for the 91500 zircon (Figure 8). Note that in the two sessions in which the NIST612 was also measured, a similar bias in measured Pb isotope ratios to the NIST614 was observed.

It is difficult to determine the bias of Pb isotope ratios observed in cassiterite due to the potential presence of common Pb. We estimate the bias to be between -0.9–+3.3% for $^{207}Pb/^{206}Pb$ in the Yankee cassiterite and between -0.4%–+2.5% in the SPG cassiterite using the most concordant data (calculated from the 2SD of the mean $^{207}Pb/^{206}Pb$ of analyses with f206c < 0.02). Note the bias of $^{208}Pb/^{206}Pb$ cannot be determined because a purely radiogenic cassiterite without Th should not have ^{208}Pb.

A systematic bias towards higher $^{207}Pb/^{206}Pb$ and $^{208}Pb/^{206}Pb$ for the 91500 zircon relative to cassiterite could explain the slightly younger ages determined for cassiterite by overcorrection of Pb isotope ratios (leading to lower corrected $^{207}Pb/^{206}Pb$ and $^{208}Pb/^{206}Pb$) when normalised to the zircon (Figure 6). The origin of a bias that is more pronounced in the 91500 zircon, and $^{208}Pb/^{206}Pb$ relative to $^{207}Pb/^{206}Pb$, in our LA-ICP-MS data is unclear. The bias per atomic mass unit is not equal between $^{207}Pb/^{206}Pb$ and $^{208}Pb/^{206}Pb$ and suggests that it is not related to IMF, but rather some matrix effect such as an unknown mass interference on ^{208}Pb that is more significant for zircon compared to the NIST glasses, or potentially an underestimation of the true $^{208}Pb^*/^{206}Pb^*$ value for the 91500 zircon. Note that a mass bias towards higher $^{207}Pb/^{206}Pb$ in zircon was also observed in SIMS U–Pb data on zircon (Stern et al. 2009). In that study, the mass bias was variable between sessions with an average offset of +0.07 ± 0.052 % ($^{208}Pb/^{206}Pb$ was not measured). Note that we do not consider the low abundance sensitivity of the systems used in this study (~80 ppm determined for mass 237 during analysis of natural U at the USGS) or inaccurate deadtime corrections for high signals, because both mechanisms will more strongly affect $^{207}Pb/^{206}Pb$ relative to $^{208}Pb/^{206}Pb$ which is contrary to the observations made here.

The 91500 zircon and NIST614 have very different Pb isotopic compositions, and the dominantly radiogenic compositions of the 91500 zircon (and cassiterite) with lower $^{207}Pb/^{206}Pb$ and $^{208}Pb/^{206}Pb$ compared to the NIST614 glass will make isotopic ratios more sensitive to analytical artifacts that overestimate ^{207}Pb or ^{208}Pb, or underestimate ^{206}Pb. Although the differences in mass bias shown are more significant for $^{208}Pb/^{206}Pb$ relative to $^{207}Pb/^{206}Pb$ it is, in fact, the $^{207}Pb/^{206}Pb$ that exerts the most control on the isochron age as analyses with lower $^{208}Pb/^{206}Pb$ (i.e., lower common Pb) are more strongly weighted in the isochron age (Figure 6). Caution is warranted when producing Pb-Pb isochron ages for cassiterite using matrix-mismatched materials as slight inaccuracies can be introduced as discussed here. Although both the NIST614 and 91500 zircon produced ages within an acceptable age range for the SPG cassiterite, we prefer the NIST614 (and NIST612) as it displays less mass bias in Pb-Pb ratios and yields ages that are more like the $^{204}Pb/^{206}Pb$ vs. $^{207}Pb/^{206}Pb$ ID-TIMS isochron age of 1540.9 ± 3.6 Ma of that sample (Tapster and Bright, 2020). However, we encourage the use of multiple reference materials with

variable Pb concentrations and compositions so that the most appropriate calibration for the unknown cassiterite sample can be used.

5.*2. Geochronology of 'young' cassiterite: U–Pb normalisation of cassiterite*

Although U–Pb ages are generally more precise compared to $^{207}Pb/^{206}Pb$ ages for samples younger than 1.5 Ga (Spencer et al. 2016), the measured $^{206}Pb/^{238}U$ ratios require large corrections for LIEF and IMF (up to 40 % and largely dependent on analytical conditions such as laser spot diameter and repetition rate) and significant inter-session reproducibility (i.e., excess variance). Since the publication of high precision ID-TIMS ages for the cassiterites used in this study, the largest source of uncertainty in U–Pb LA-ICP-MS ages comes from the excess variance of $^{206}Pb^*/^{238}U$ of the primary reference material; estimated to be ±1.9%.

.2.1. Matrix-mismatched reference materials

Matrix-mismatched reference materials have been employed in U–Pb cassiterite geochronology due to the inaccessibility of quality matrix-matched reference materials (Blevin and Norman, 2010b; Yuan et al., 2011; Oberthür et al., 2016; Cheng et al., 2019; Kendall-Langley et al., 2020; Gemmrich et al., 2021; Marcoux et al., 2021).

Neymark et al. (2018) document a matrix bias yielding U–Pb ages *ca* 12 and 15% older in cassiterite when $^{238}U/^{206}Pb$ is normalised to the NIST612 using a laser spot size between 85 and 135 µm and a repetition rate of 5 Hz and energy density of 5 J/cm^2. In that study, the larger laser spot size (135 µm) also produced older apparent ages (higher corrected Pb/U). Cheng et al. (2019) use the NIST610 glass for U–Pb normalisation of cassiterite and using spot sizes of 44–58 µm, laser fluence of 4 J/cm^2, a laser repetition rate of 10 Hz, and tuning of the LA-ICP-MS system such that the $^{206}Pb/^{238}U$ ratio obtained at the start of ablation was similar to the reference value for the NIST610 glass. In this study, we show that when used as a reference material, the NIST614 yields U–Pb ages that are systematically too young for all cassiterites (Figure 7). The 2SD uncertainty of U–Pb ages for 3 analytical sessions at GeoRessources where NIST614 was used for normalisation of Pb/U was equal to or greater than when when using cassiterite reference materials. Two studies have normalised $^{238}U/^{206}Pb$ in cassiterite to the 91500 zircon as a matrix mismatched reference material (Yuan et al., 2011; Oberthür et al., 2016), whilst Neymark et al. (2018) suggest this method introduces *ca* 7% bias towards older U–Pb ages. In this study, two analytical sessions yield U–Pb ages 0.4 and 2% younger than the accepted values of the cassiterite samples (Figure 7), whilst the third session yield an age 8% older. The variable older and younger bias noted in here and in other studies when using either the NIST612 (or NIST614) or zircon matrix-mismatched reference materials, indicates a high degree of

sensitivity of laser parameters and instrument tuning to the matrix-bias between the NIST glasses and zircon for U–Pb cassiterite geochronology. In Figure 7, the analytical sessions 7025 and 7465 used a laser spot size of 95 µm, 5Hz repetition rate and 5J/cm^2 energy density, whilst session 7490 used a 95µm spot size, 8 Hz repetition rate and 3J/cm^2 energy density. Therefore, the difference observed between ages from session 7025 and 7465 compared to 7490 may be due to downhole fractionation.

Downhole fractionation of U and Pb is considered the most dominant mechanism leading to biased Pb/U ratios in zircon geochronology by LA-ICP-MS (Paton et al., 2010). The time-resolved variations of $^{206}Pb/^{238}U$ in cassiterite, NIST614 glass and the 91500 zircon with three different laser ablation configurations are compared in Figure 9A, and the relative change in $^{206}Pb/^{238}U$ with time in Figure 9B. Cassiterite and the NIST614 show a linear evolution of $^{206}Pb/^{238}U$ with time, with cassiterite yielding a slightly positive trend in samples without significant common Pb compared to the negative trend of the NIST614. Time resolved Pb/U of the 91500 zircon is defined by logarithmic functions for all laser parameters. The differential trend in downhole fractionation of $^{206}Pb/^{238}U$ between the NIST614, 91500 zircon and cassiterite means that these matrix-mismatched reference materials will produce variably inaccurate U–Pb cassiterite ages depending on the aspect ratios of the ablation pits. For the largest aspect ratio shown in Figure 9A (Laser parameters: 70 µm spot size, 5 Hz laser repetition rate and 5 J/cm² laser density), the downhole corrected mean $^{206}Pb/^{238}U$ of the Yankee cassiterite is 5.9% higher (or age is 5.9% older) than the true value when normalised to the NIST614 model, and 5.6% lower (or younger) than the true value when normalised to the 91500 zircon model. For the smallest aspect ratio in Figure 9A (Laser parameters: 35 µm spot size, 8 Hz and 5 J/cm²), the downhole corrected mean $^{206}Pb/^{238}U$ of the Yankee cassiterite is 3.5% higher (or 3.5% older) than the true value when normalised to the NIST614 model, and 11% lower (or younger) when using the 91500 zircon model. Differential $^{206}Pb/^{238}U$ downhole fractionation models of $^{206}Pb/^{238}U$ between the 91500 zircon and cassiterite and NIST614 and cassiterite can explain younger and older cassiterite ages, respectively, shown in Neymark et al. (2018), but not in GeoRessources dataset which shows a more varied relationship.

Therefore, some process in addition to LIEF of U-Pb seems necessary to explain the matrix biases noted in these data when U–Pb ratios of cassiterite are normalised to synthetic glasses or zircon. A possibility is variable mass load on the plasma related to the widely different ablation efficiencies and densities of the cassiterite (*ca* 7 g/cm^3), zircon (*ca* 4.6 g/cm^3) and glass (*ca* 2.5 g/cm^3) matrices (e.g., Kroslakova and Günther, 2007b). Mass load effects can produce variable intensity ratios for volatile/refractory elements, possibly through incomplete vaporization of ablated particles (e.g., Guillong et al., 2003; Yu et al., 2003) or element-dependent ionization structures within the plasma (Kroslakova and Günther, 2007b; Fietzke and Frische, 2016). Fietszke and Fritch

(2016) predict strong matrix effects related to mass load on the plasma when the sample represents more than 1% of the total aerosol (i.e., the remaining 99% of the aerosol is Ar and He gas) and this limit can be surpassed with the ablation parameters (spot size, repetition rate) commonly used in LA-ICP-MS geochronology of cassiterite. Mass load effects are problematic when using different laser spot sizes or repetition rates on a similar matrix, but they are potentially even more significant when normalising to matrix-mismatched reference materials with significantly different densities and ablation characteristics. For example, Si-rich synthetic glasses such as NIST612 ablate at twice the rate of cassiterite due to their different material densities and laser absorptivities (Neymark et al., 2018) and this large difference will result in very different quantities of material arriving at the plasma source. The relative ablation rates of a zircon and cassiterite are unavailable; here we considered them to be similar because the NIST610 glass ablates approximately 1.5 times faster compared to the 91500 zircon (Kuhn et al., 2010b), and the NIST612 glass ablates approximately 2 times faster than cassiterite (Neymark et al., 2018). Such matrix effects can be mitigated somewhat by optimizing experimental conditions such as sampling depth of the plasma (e.g., Yu et al., 2003), removing large particles (Guillong et al., 2003), or diluting the ablation stream before it enters the plasma (Kroslakova and Günther, 2007b). Unfortunately, it is difficult to generalise laser and ICP-MS parameters that prevent mass load effects, as these will vary between instrument systems and mineral matrices. Cassiterite U–Pb geochronology often requires substantially larger spot sizes in order to increase ^{207}Pb signal intensity, which will increase the likelihood of mass load effects when using the NIST glasses for IMF corrections. However, it may be difficult to explain the contrasting behaviour of U–Pb between different labs noted here (e.g., older vs. younger apparent ages in the USGS vs. GeoRessources data) by any single process and further work is required to better understand possible matrix effects in LA-ICPMS geochronology.

Matrix-mismatched reference materials appear to produce accurate U–Pb ages under certain analytical conditions, although these conditions are not applicable for all studies or samples. In U–Pb geochronology, mass load effects may be more influential when using larger spot sizes and synthetic glasses for ^{238}U/^{206}Pb normalisation, whilst down-hole fractionation will be more important when using smaller spot sizes and a zircon for ^{238}U/^{206}Pb normalisation. Therefore, we suggest that in the absence of matrix-matched reference materials, that a NIST glass is more appropriate for smaller spot sizes (i.e.. <50 µm) and zircon for larger spot sizes (>50 µm) and common laser repetition rates (5 Hz) and fluence (5 J/cm^2). However, there are large uncertainties in the reproducibility of both methods as demonstrated here, and preference should be given to matrix-matched reference materials when available. Older cassiterite U–Pb ages can be verified using the Pb-Pb ages of the same samples, however, younger cassiterite requires other independent geochronological constraints to verify U–Pb ages determined using matrix-

mismatched materials. Note that operating conditions of the ICP-MS (e.g., the distance between sampler cone and the load coil and/or carrier gas flow rate) can also influence the transmission of elements (e.g., Yu et al., 2003), but these conditions were not investigated here.

5.2.2. Matrix matched reference materials

Normalisation of U–Pb ratios using matrix-matched reference materials is currently the most accurate method for LA-ICP-MS geochronology of cassiterite younger than *ca* 1.5 Ga. U–Pb ages determined here using the SPG, Yankee, AY-4 and Jian-1 cassiterite for normalisation of $^{238}U/^{206}Pb$ each yield ages that are mostly comparable to each other and relative to the independently determined ages of those cassiterites (Figure 5; Appendix B). The U–Pb age of the AY-4 after normalisation to the SPG, Yankee and Jian-1 suggests a crystallisation age of *ca* 154 Ma (Table 3) that is similar to a recent ID-TIMS age 154.3 ± 0.7 Ma (Yang et al. 2022*)* but not with two previous ID-TIMS ages of 151.9 ± 1.5 Ma (Carr et al., 2020) and 158.2 ± 0.4 Ma (Yuan et al., 2011). The reason for the discrepancy between the ID-TIMS ages of these two earlier studies is unclear but could be related to analytical bias within the ID-TIMS data or the use of inappropriate common Pb compositions as suggested by Yang et al. (2022), or real age variability within the splits used for these analyses.

In this study, the novel method for normalisation without high precision ID-TIMS data of cassiterite presented by Neymark et al. (2018) yields similar U–Pb ages to conventional methods. The minor bias in LA-ICP-MS $^{208}Pb/^{206}Pb$–^{207}Pb-^{206}Pb isochron ages observed when using the 91500 zircon for normalisation of Pb-Pb isotopes (as discussed previously) should be considered. Although this bias is small, it highlights the necessity of appropriate age uncertainty propagation in LA-ICP-MS U–Pb geochronology to account for analysis induced bias.

5.3 A note on common Pb corrections

Common Pb corrections or anchored Discordia can introduce bias in U–Pb cassiterite ages by incorrectly assuming the common Pb composition (by terrestrial earth Pb evolution models such as Stacey and Kramers, 1975 or within associated low U minerals) as discussed in Tapster and Bright (Tapster and Bright, 2020) and documented in Carr et al. (2020), Neymark et al. (2021b) and Yang et al. (2022). This bias is most important for high precision ID-TIMS studies; however, it can potentially introduce inaccuracies within LA-ICP-MS data that are outside the total uncertainty if the assumed common Pb composition is significantly different from the true composition. For example, Carr et al. (2020) determined a $^{207}Pb/^{206}Pb_i$ of 0.74 ± 0.10 from the upper intercept of a 'Total Pb' isochron of ID-TIMS data that was later reproduced by Yang et al., (2022) with a value of 0.722 ± 0.075 from the upper intercept of a $^{207}Pb/^{206}Pb$ vs. $^{238}U/^{206}Pb$ Discordia of LA-ICP-MS data. The value predicted

by Stacey and Kramers (1975) terrestrial Pb evolution model for the Earth of 0.852 ± 0.017 is significantly higher than the original ID-TIMS estimate. However, in this study the $^{207}Pb/^{206}Pb_i$ values range between 0.69 ± 0.03 and 0.95 ± 0.03 and suggest heterogeneity in common Pb composition of the Yankee cassiterite. Fortunately, the large number of concordant and near concordant analyses that are typical to the Yankee cassiterite restrict the influence of this variable common Pb on the lower intercept age. However, caution is warranted particular for samples with only moderate to high common Pb (e.g., f206c > 0.1) and poor dispersion along the Discordia.

Despite these drawbacks, common-Pb corrected ages and mean weighted $^{206}Pb^*/^{238}U$ ages can be reported for cassiterite geochronology (e.g., Zhang et al., 2017). Common-Pb corrections can be applied to raw data prior to processing (e.g., Zack et al., 2011) or data already treated for the effects of LIEF and IMF (e.g., Chew et al., 2014). An example of the effect of different common Pb corrections on ages is shown in Appendix E for the Jian-1 cassiterite (after normalisation to the SPG and NIST614). The lower intercept age for these data uncorrected for common Pb is 152.0 ± 1.4 (3.1) Ma with an MSWD of 1.7. We applied ^{207}Pb- and ^{208}Pb- common Pb corrections (using $^{207}Pb/^{206}Pb_i$ = 0.846 ± 0.005, $^{208}Pb/^{206}Pb_i$ = 2.08 ± 0.04 and $^{208}Pb/^{207}Pb_i$ = 2.46 ± 0.04) to determine mean weighted $^{206}Pb^*/^{238}U$ ages of 153.2 ± 1.3 (3.0) Ma with an MSWD of 3.3 and 149.5 ± 1.3 (3.0) Ma with an MSWD of 1.8, respectively. Applying the ^{208}Pb-correction to the raw data as described by Zack et al., (2011) yields an age of 151.2 ± 1.5 (3.1) with an MSWD of 2.3. We also tested the ^{208}Pb-correction on raw data not already treated for LEIF and IMF (as described in Zack et al., 2011) on $^{207}Pb^*/^{206}Pb^*$ ages for the SPG assuming $^{208}Pb/^{206}Pb_i$ = 2.22 ± 0.05 and $^{208}Pb/^{207}Pb_i$ = 2.32 ± 0.04. The session lower intercept age was 1538.7 ± 6.8 (8.5) Ma (Appendix D) that is within uncertainty of the mean weighted $^{207}Pb^*/^{206}Pb^*$ age of 1533.7 ± 6.3 (44) Ma. The larger uncertainty of the $^{207}Pb^*/^{206}Pb^*$ is due to the added uncertainty from the $^{208}Pb/^{206}Pb_i$ and $^{208}Pb/^{207}Pb_i$ values. In summary, common Pb corrections may provide marginal improvement in precision, although inappropriate common Pb compositions can induce bias and excess scatter of mean weighted $^{206}Pb^*/^{238}U$ ages. $^{207}Pb^*/^{206}Pb^*$ ages of Precambrian cassiterite such as the SPG will generally be less precise compared to $^{208}Pb/^{206}Pb$–^{207}Pb-^{206}Pb isochron ages due to the uncertainty of the common Pb values used.

Therefore, and whenever possible, U–Pb ages of common-Pb bearing cassiterite are better determined by Disocordia relationships in classic $^{207}Pb/^{206}Pb$ vs. $^{238}U/^{206}Pb$ or $^{236}Pb/^{238}U$ vs. $^{207}Pb/^{235}U$ diagrams (Tapster and Bright, 2020). If data populations do not contain concordant analyses to ‘fix’ the lower intercept age, then age bias is more susceptible to the common Pb composition selected.

5.4. Characteristics of cassiterite reference materials

The SPG cassiterite represents a U-rich and Th-poor example of Precambrian age with a precise U–Pb ID-TIMS age (Tapster and Bright, 2020). The SPG cassiterite is available for interested laboratories (contact L.A. Neymark for more details). The available grain sizes are *ca* 0.1-0.2 mm in diameter. The SPG has a wide range in U mass fraction between *ca* 5 and 230 µg/g, and analytical protocols need to accommodate this large range (for example, we use ^{235}U to estimate ^{238}U when cps of the latter are greater than $2.5x10^6$). Despite the relatively low $^{238}U/^{206}Pb^*$ of the SPG (~3.5), the SPG-based normalisation produces reliable ages of Phanerozoic cassiterite with much higher $^{238}U/^{206}Pb^*$ (Neymark et al., 2018; 2021b). Precambrian cassiterites with high U and homogenous U–Pb isotopic compositions and low common Pb such as the SPG are unsurprisingly rare in the literature as about 90% of hard-rock and alluvial tin production originates from deposits that are <350 Ma (Lehmann, 2020). Except the SPG, two Archean pegmatites in the Pilbara Craton, Western Australia, that have moderate U, low Th, low common Pb and a ^{207}Pb-^{206}Pb age of ca 2850 Ma are the other Precambrian cassiterite with favourable characteristics for use as a reference material that have been currently published (Kendall-Langley et al., 2020; Denholm et al., 2021). In addition, Precambrian cassiterite from tin deposits in Brazil (Rondônia and Pitinga tin provinces) and South Africa (related to Archean Bushveld complex) (Neymark et al., 2018; Yang et al., 2022) can be further investigated as potential reference materials.

The Yankee cassiterite is available for interested laboratories (contact P.A. Carr for more details). The available grain sizes are between 0.3 and 3 mm in diameter. The Yankee cassiterite has a well-defined by ID-TIMS U–Pb age of 246.48 ± 0.51 Ma (Carr et al., 2020). The low U mass fraction of the Yankee cassiterite means that adequately precise determination of ^{207}Pb can be analytically challenging, and a laser spot diameter of >60 µm is generally required. Due to the variable common Pb that is found within the Yankee, the 207-common Pb correction requires relatively precise $^{207}Pb/^{206}Pb$, particularly when f206c>0.05. Despite this potentially greater uncertainty of $^{207}Pb/^{206}Pb$ and variable common Pb, we show here that the Yankee cassiterite can yield accurate results for Precambrian and Phanerozoic cassiterite when used for normalisation of U–Pb ratios.

AY-4 is commonly used as a reference material for U–Pb dating of cassiterite by LA-ICP-MS. The U mass fraction of this cassiterite is highly variable (17–330 µg/g). We achieve the best results using the most recently reported ID-TIMS U–Pb age of 154.3 ± 0.7 Ma (Yang et al. 2022), however, we cannot exclude age heterogeneity in the distributed AY-4.

The Jian-1 cassiterite is not available for distribution. Certains grains of the Jian-1 contain very little U (1–5 µg/g) and will result in greater uncertainties, particularly for $^{207}Pb^*/^{206}Pb^*$. However, the *ca* 155 Ma age of the Jian-1 and AY-4 cassiterite is particularly interesting as it is like many other cassiterite deposits around the world

including other Mesozoic deposits of South China, and the Malaysia and Indonesia that make up 60–65% of the worlds historical production (Lehmann, 2020).

We note that other well-defined reference materials are those reported in Tapster and Bright (2020) and Yang et al. (2022).

6. Conclusions

We have compared key compositional parameters of four cassiterites that have been used as reference materials in previous U–Pb geochronology studies (SPG, Yankee, AY-4, and Jian-1) and determined the relative accuracy of each cassiterite for normalisation of $^{238}U/^{206}Pb$ ratios during *in situ* LA-ICP-MS U–Pb age determinations. We also tested the suitability of the matrix-mismatched reference materials of the NIST614 and NIST612 synthetic glasses and the 91500 zircon for their applicability as normalising reference materials for cassiterite geochronology.

$^{208}Pb/^{206}Pb$–^{207}Pb-^{206}Pb isochron ages are advantageous for dating > 1.5 Ga low-Thcassiterite such as the SPG by LA-ICP-MS due to the minor matrix effect on instrumental mass fractionation of Pb isotopes. We note a 0.6% bias introduced in these ages of the SPG when using the NIST614 and NIST612 (1539.7 ± 6.1 (8.0) Ma) vs. 91500 zircon (1531.1 ± 7.1 (8.68) Ma) matrix-mismatched reference materials for normalisation of Pb-isotope ratios. We conclude that ideally reference materials with similar Pb concentration and composition should be used for normalisation of Pb-Pb ratios.

U–Pb ratios derived from normalisation to matrix-mismatched reference materials such as the NIST glasses or 91500 zircon show varied results in this study and within the literature. Certain analytical conditions may permit the use of matrix mismatched reference materials; however, those conditions are poorly defined and may vary between LA-ICP-MS systems. Ideally, U–Pb ratios are best normalised to matrix-matched reference materials such as the Yankee, SPG, Jian-1 or AY-4 cassiterite. The U–Pb ages of *ca* 1535 for the SPG, *ca* 245 Ma for the Yankee, and *ca* 155 Ma for the Jian-1 and AY-4 cassiterite are equally obtained when any of those cassiterites are used for normalisation of $^{238}U/^{206}Pb$ indicating internal consistency in their assumed ages. The use of these well characterized matrix-matched reference materials such as those presented in this study can now permit LA-ICP-MS U–Pb cassiterite ages that approach the long-term reproducibility achieved in *in situ* zircon geochronology (*ca* 1.9 % in cassiterite; this study, and *ca* 1.5 % in zircon; e.g., Hortswood et al., 2016) and permit greater confidence in accuracy of the presented ages and more realistic uncertainties

Supplementary Materials:

Appendix A1: U–Pb isotopic data of cassiterite and normalisation to the Yankee, SPG and Jian-1 cassiterite for U–Pb and the 91500 zircon, NIST612 and NIST614 glasses for Pb-Pb.

Appendix A2: U–Pb isotopic data of cassiterite and normalisation to the the 91500 zircon and NIST614 glasses for U–Pb and Pb-Pb.

Acknowledgments: P.C. was funded by Institut Carnot ICEEL and the French National Agency through the national programme "Investissements d'avenir" of the Labex Ressources 21 (Reference ANR-10-LABX-21-RESSOURCES21). This research was funded by an OSU OTELo grant to J.M. "Développement du traçage géochimique et de la datation U-Th-Pb *in situ* des colombo-tantalites, cassitérites et wolframites par couplage LA-ICP-MS et SIMS" and a CNRS-INSU-CESSUR grant (AO INSU TELLUS call) to J.M. "développement du traçage géochimique et de la datation U-Th-Pb *in situ* Colombo-tantalites, cassitérites et wolframites par couplage LA-ICP-MS et SIMS". The laser ablation and ICP-MS used in this study at GeoRessources were funded from a grant received from the 'Plan Etat Région', the Région Lorraine, and Labex Ressources 21. We would like to thank Chris Holm-Denoma and Kate Souders for their help in optimizing LA-ICP-MS system at USGS. The Yankee cassiterite was provided by P.L. Blevin and the AY-4 used in this study was provided R.Q. Zhang. We gratefully acknowledge A. Larin of the Institute of Precambrian Geology and Geochronology, Saint Petersburg, Russia for providing Pitkäranta cassiterite samples for this study. This manuscript benefited from the editorial handling of Thomas Zack and Ed Williams and two anonymous reviews. A previous version of this manuscript was also improved by comments from Michel Cuney, Simon Tapster, and an anonymous reviewer. Any use of trade, firm, or product names is for descriptive purposes only and does not imply endorsement by the U.S. government.

Figures and captions

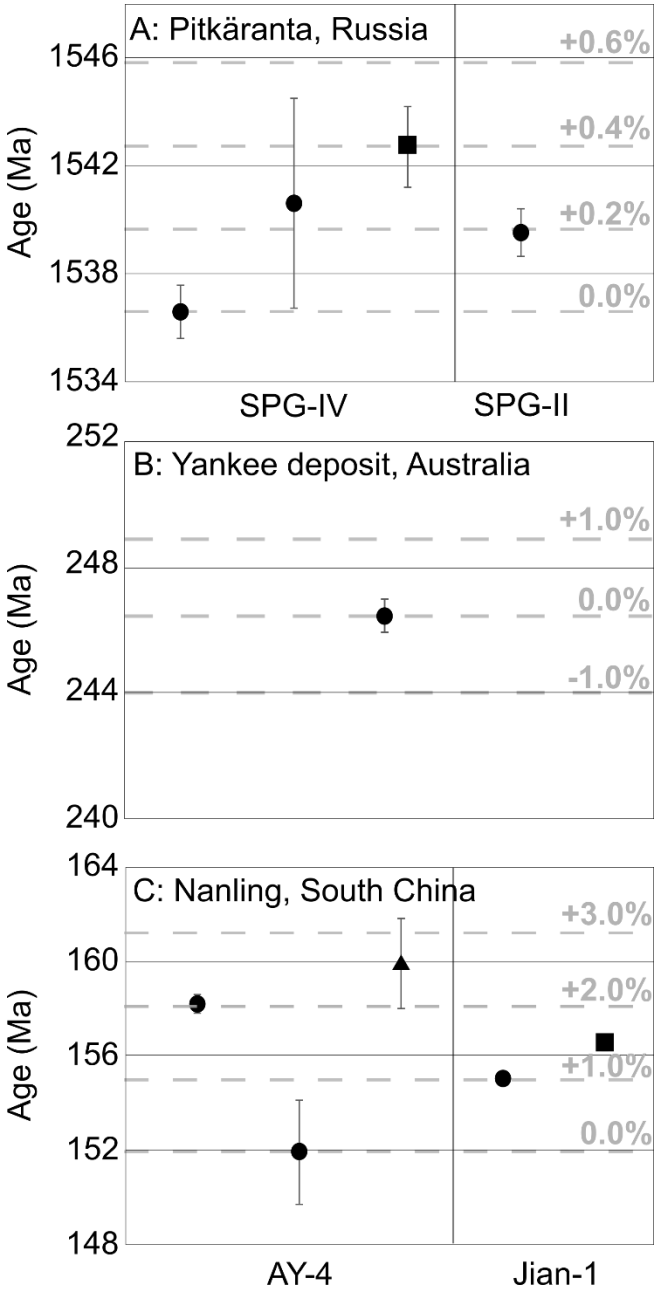

Figure 1. Published U–Pb ages for cassiterite reference materials determined from A) the Pitkäranta ore district, Russian Karelia (ages for two aliquots of sample SPG from left to right; relative uncertainty in parentheses: 1536.6 ± 1.0 (0.07%) Ma (Tera-Wasserburg lower intercept age or T-W age), 1540.9 ± 3.6 (0.2%) Ma ($^{204}Pb/^{206}Pb$ vs. $^{207}Pb/^{206}Pb$ isochron age) (Tapster and Bright, 2020), 1542.7 ± 1.5 (0.10%) Ma (mean weighted $^{208}Pb/^{206}Pb$ vs. $^{207}Pb/^{206}Pb$ isochron age) (Neymark et al., 2018) and 1539.5 ± 0.9 (0.06%) (Concordia intercept age) (Rizvanova and Kuznetsov, 2020), B) the Yankee lode, Eastern Australia: 246.48 ± 0.51 (0.20%) Ma (Carr et al., 2020) ('Total Pb' isochron age), and C) the Nanling Range, South China including the AY-4: 158.2 ± 0.4 (0.25%) Ma (mean weighted $^{206}Pb^*/^{238}U$ age) (Yuan et al., 2011), 151.9 ± 2.2 (1.44%) Ma ('Total Pb' isochron age) (Carr et al., 2020) and 159.9 ± 1.9 (1.20%) Ma ($^{206}Pb/^{207}Pb$ vs. $^{238}U/^{207}Pb$ isochron age) (Yuan et al., 2011)

and the Jian-1: 154.969±0.082 (0.05%) Ma (T-W age) (Tapster and Bright, 2020) and 156.55 ± 0.36 Ma (0.23%) (T-W age) (Neymark et al., 2018). Symbols represent the method used for age determination: circle = ID-TIMS, square = LA-ICP-MS, triangle = LA-MC-ICP-MS.

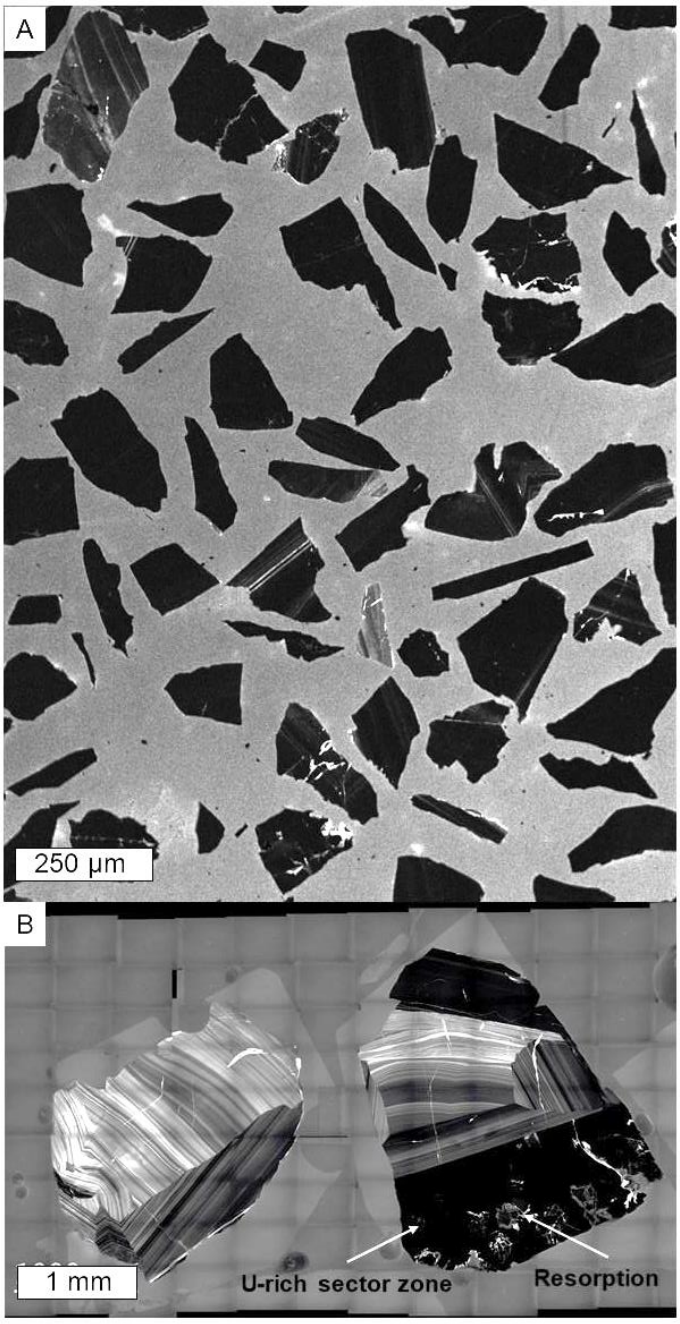

Figure 2: Cathodoluminescent images of cassiterite from (A) the SPG, Pitkäranta ore district, Russian Karelia showing very little CL response and (B) the best quality crystals with minor alteration of primary textures of Yankee lode, eastern Australia (B).

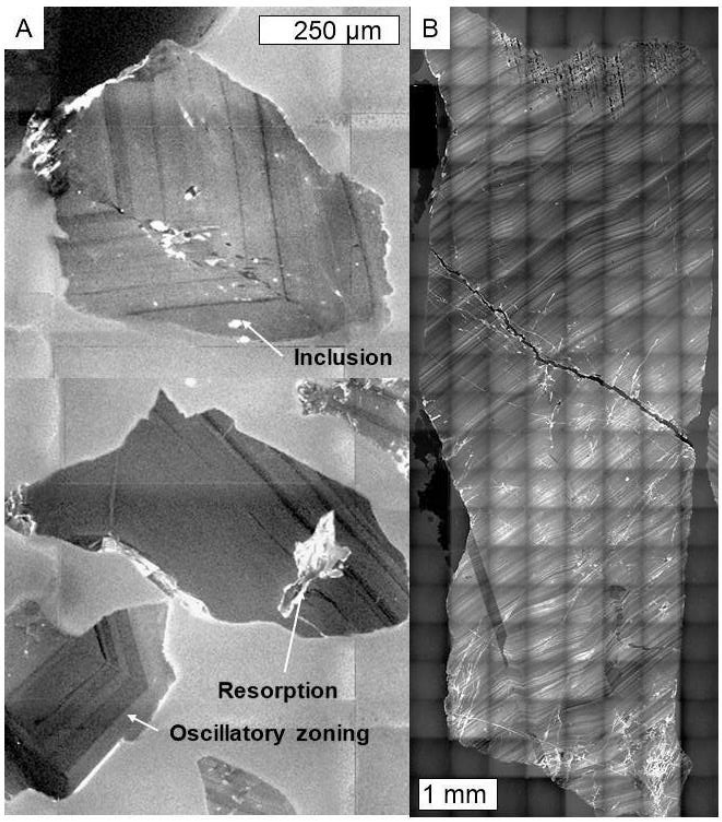

Figure 3: Cathodoluminescence images of the AY-4 (A) and Jian-1 (B) reference cassiterite.

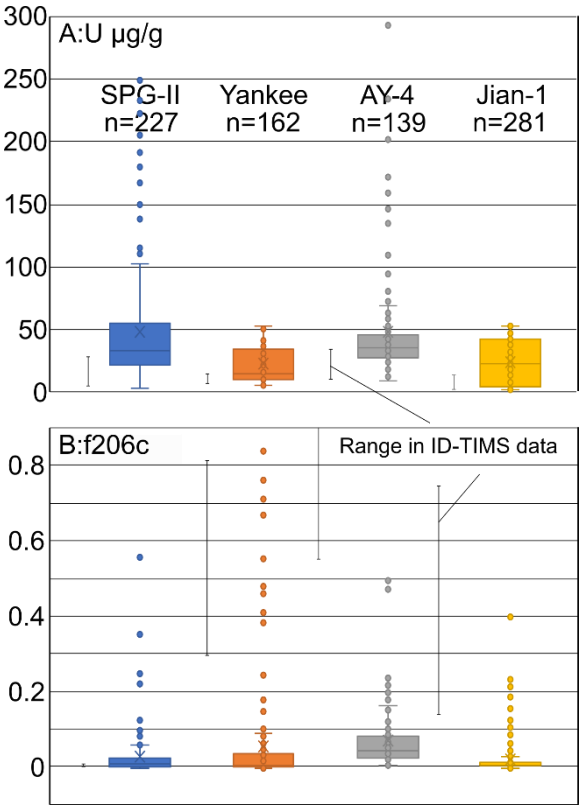

Figure 4. Box and whisker plot showing key parameters for the cassiterite used in this study including A) U mass fraction (in µg/g), B) proportion of common Pb (f206c; see equation 1 in text). The "X" marks the median value. The range in U mass fraction and f206c (Carr et al., 2020; Tapster and Bright, 2020) of ID-TIMS data for the same samples are shown in A and B. ID-TIMS data of AY-4 originates only from Carr et al. (Carr et al., 2020) as these are not reported in Yuan et al. (Yuan et al., 2011)

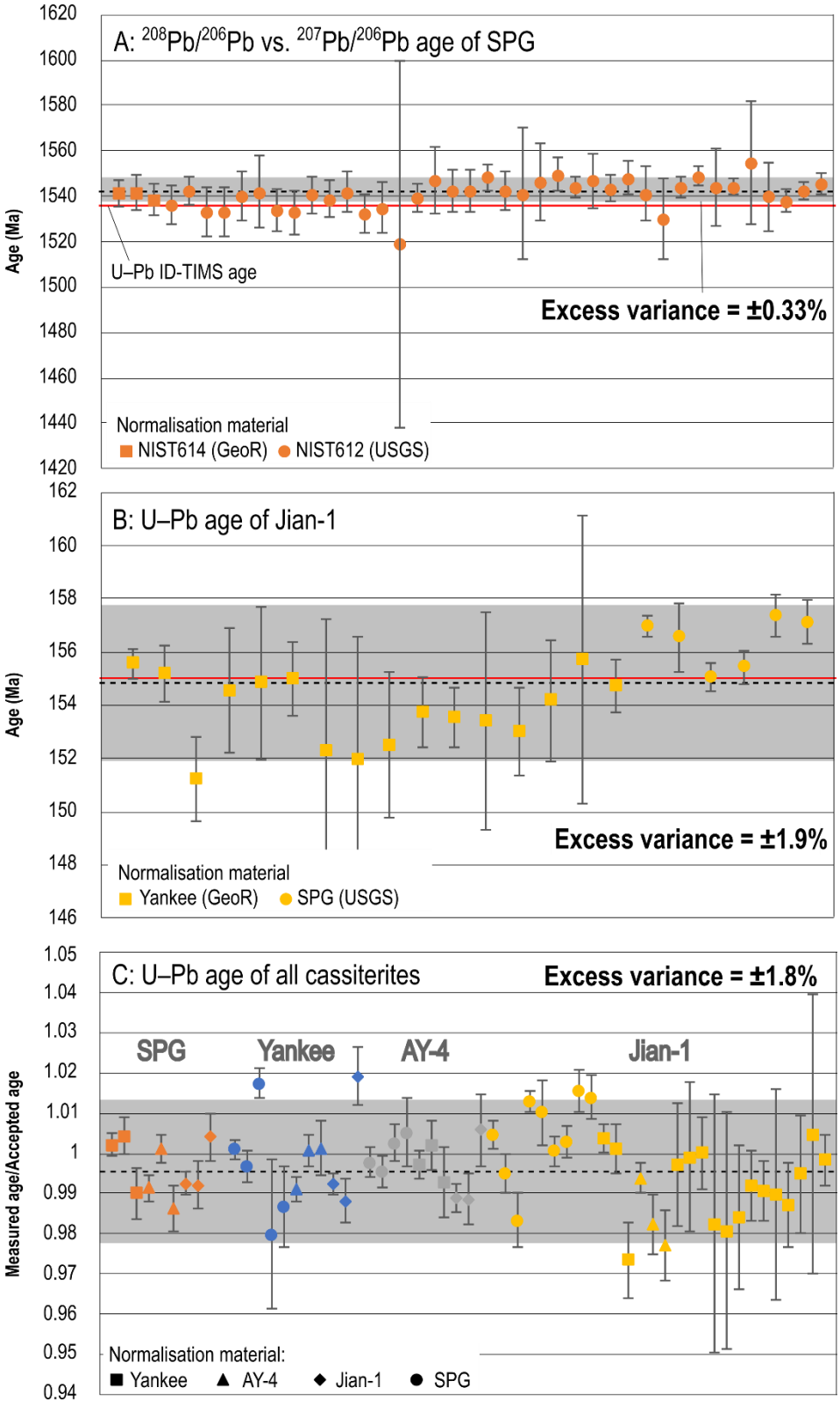

Figure 5. Excess variance of $^{208}Pb/^{206}Pb$–$^{207}Pb/^{206}Pb$ isochron ages of the SPG (A) and U–Pb ages of the Jian-1 using the different normalisation methods of GeoRessources and USGS (see Section 3.2). The ID-TIMS ages for those samples are represented by the red line. All measured cassiterite ages normalised to their accepted age are shown in (C).

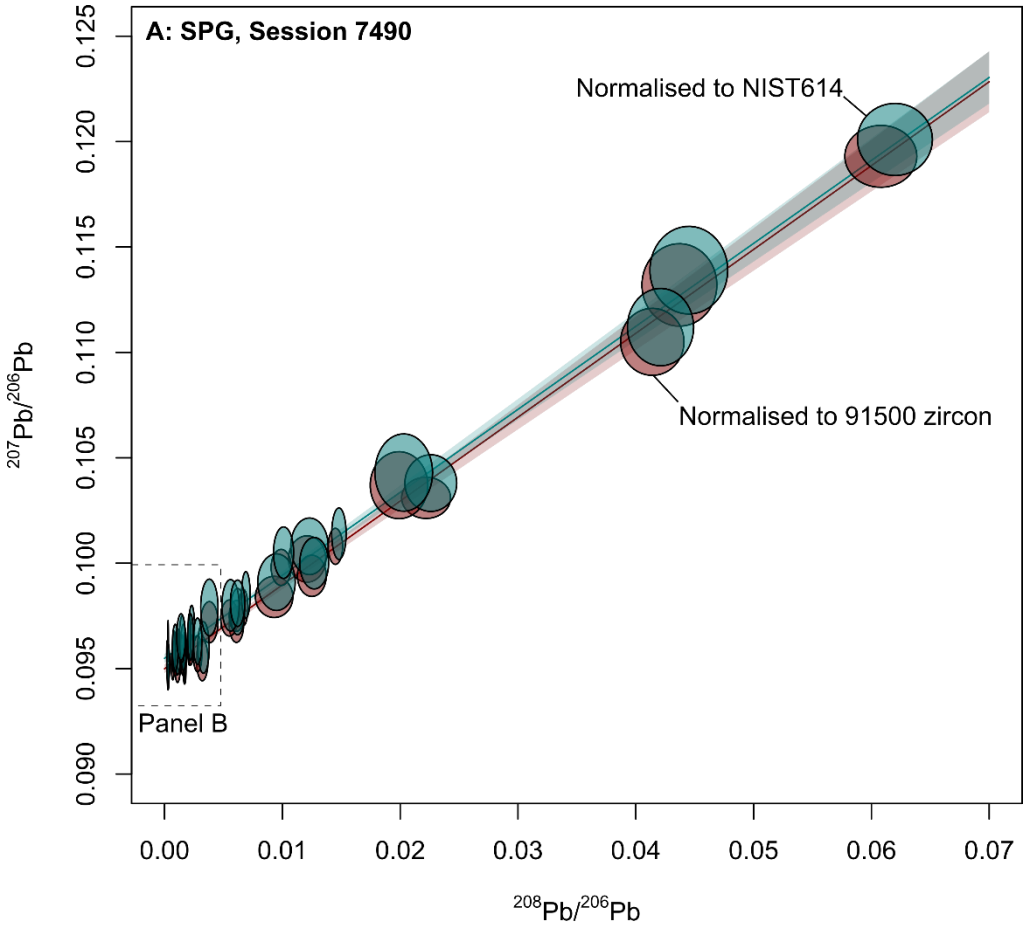
A: SPG, Session 7490
Normalised to NIST614
Normalised to 91500 zircon
Panel B
$^{207}Pb/^{206}Pb$
$^{208}Pb/^{206}Pb$
0.090
0.095
0.100
0.105
0.110
0.115
0.120
0.125
0.00
0.01
0.02
0.03
0.04
0.05
0.06
0.07

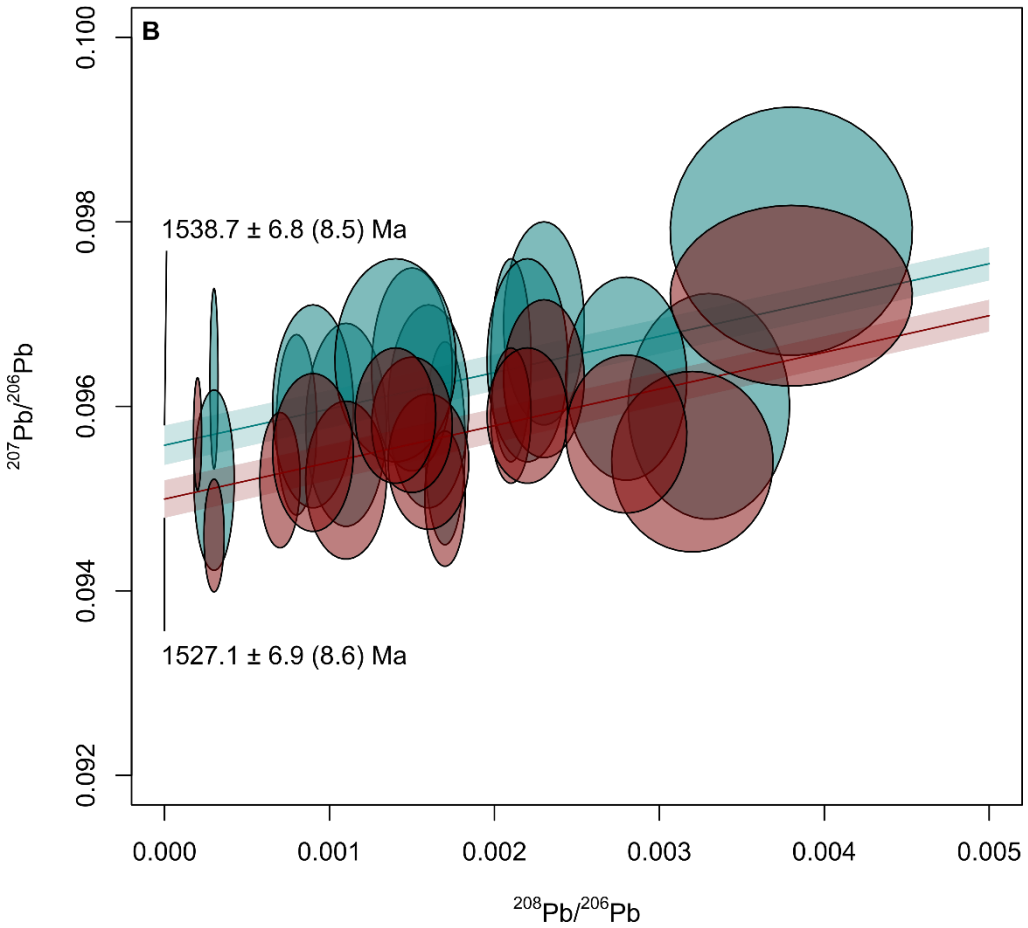
B
1538.7 ± 6.8 (8.5) Ma
1527.1 ± 6.9 (8.6) Ma
$^{207}Pb/^{206}Pb$
$^{208}Pb/^{206}Pb$
0.092
0.094
0.096
0.098
0.100
0.000
0.001
0.002
0.003
0.004
0.005

Figure 6: $^{208}Pb/^{206}Pb$–$^{207}Pb/^{206}Pb$ isochron ages of SPG cassiterite normalised to the NIST614 glass (teal) and 91500 zircon (dark red) in a single session. C) Enlarged panel from A showing isochron ages.

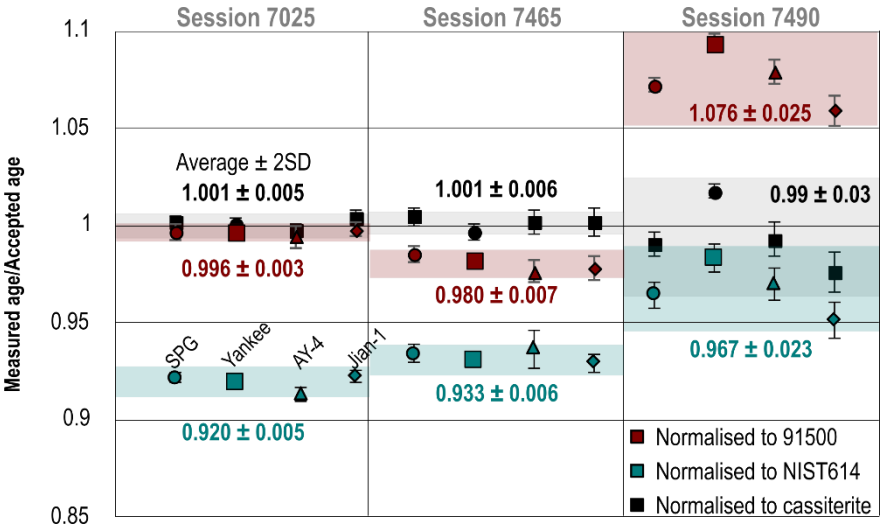

Figure 7: Measured/Accepted U–Pb lower intercept ages for all cassiterite and normalised to the 91500 (maroon infill), NIST614 (teal infill) and cassiterite (black infill). Cassiterite data are normalised to the Yankee cassiterite, except the Yankee cassiterite itself that is normalised to the SPG. The average and 2SD for each analytical session are marked for each session and normalisation material. Data are from three analytical sessions from GeoRessources (Sessions 7025,7465 and 7490). Laser parameters for each session as follows: 7025 and 7465; 95 µm spot diameter, 5 Hz repetition rate, 5 J/cm^2; 7490; 95 µm, 8Hz and 3 J/cm^2.

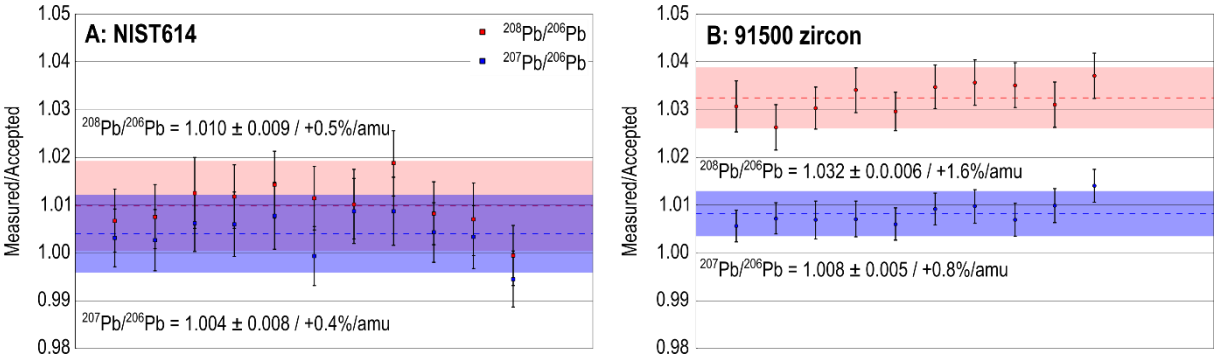

Figure 8: Measured/Accepted Pb/Pb values for the NIST614 (A) and 91500 zircon (B) for a single analytical session (Session 7025). $^{208}Pb/^{206}Pb$ are shown in red, and $^{207}Pb/^{206}Pb$ in blue. The average value and 2SD uncertainty are presented by the dashed line and shaded area for each ratio.

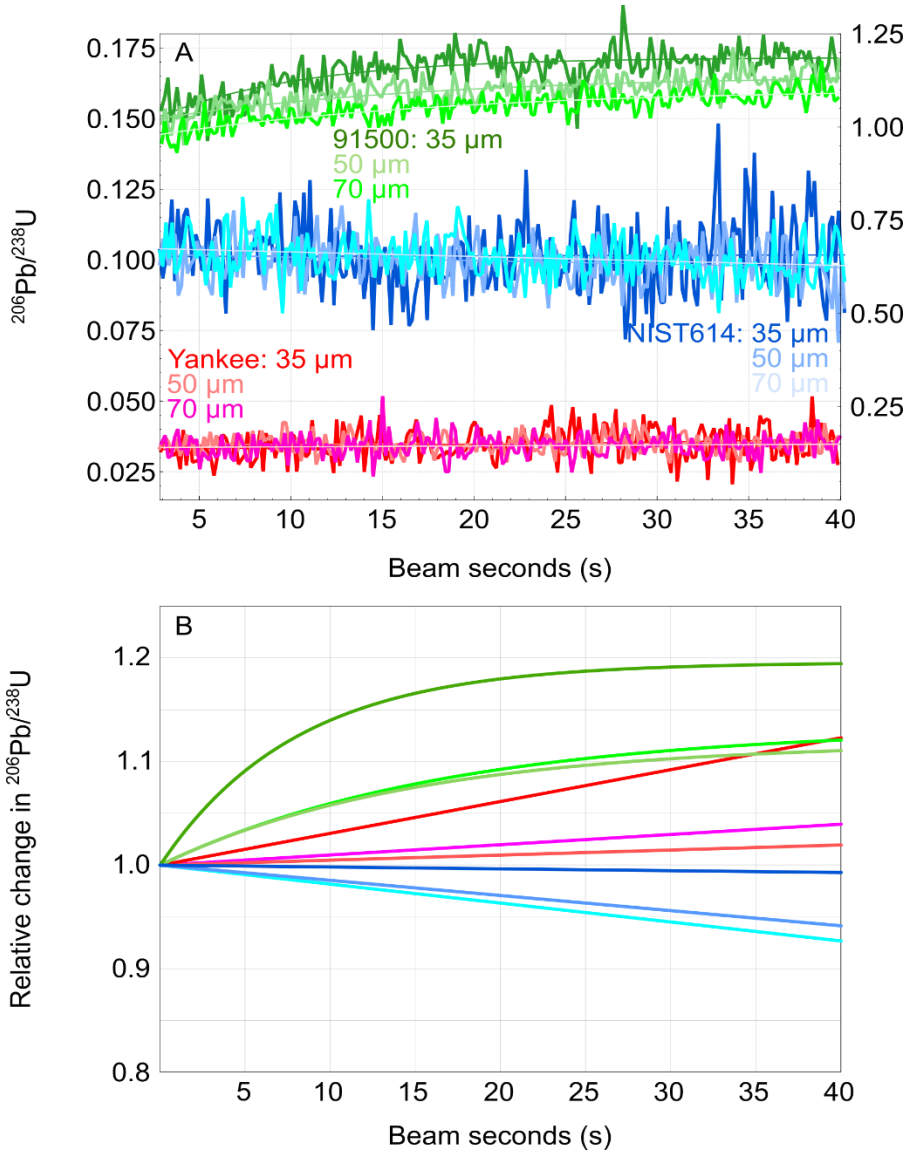

Figure 8: A) Time-resolved $^{206}Pb/^{238}U$ and downhole fractionation models of cassiterite (SPG, Yankee, Jian-1 and AY-4), zircon (91500) and synthetic glass (NIST614) matrices for three different laser ablation parameters: 1) 70 µm, 5Hz, and 5Jcm², 2) 50 µm, 8 Hz, and 5Jcm², and 3) 35 µm, 8 Hz and 5Jcm². B) Relative change in $^{206}Pb/^{238}U$ during ablation for all materials shown in A and based on linear (for NIST614 and Yankee cassiterite) logarithmic functions (91500 zircon).

Tables

Table 1. Analytical setup and parameters for U–Pb LA-ICP-MS of cassiterite

Laboratory	**GeoRessources**	**USGS**
Mass spectrometer	AttoM (ES) SF-ICP-MS	
Laser system and cell:	ESI 193 nm ArF excimer laser ablation system with two-volume 'TwoVol2' sample cell	Teledyne Photon Machines Excite-Analyte™ 193 nm ArF excimer laser ablation system with two-volume HelEx sample cell
Mass spectrometer parameters:		
RF generator power:	1300 W	
Acceleration voltage:	6000 V	
Coolant gas:	13.0 L min^{-1}	
Auxiliary gas:	0.9–1.0 L min^{-1}	
Instrument resolution mode:	300 (low)	
Analysis mode	Deflector jump	
Acquisition mode	Time resolved analysis	
Peak center mass	None	^{206}Pb
Peak integration times (per sweep):	^{202}Hg (500 µs), ^{204}Pb (500 µs) ^{206}Pb (500 µs), ^{207}Pb (1.5 ms) ^{208}Pb (500 µs), ^{232}Th (500 µs) ^{235}U (500 µs), ^{238}U (500 µs).	^{202}Hg (500 µs), ^{204}Pb (500 µs), ^{206}Pb (500 µs), ^{207}Pb (1.5 ms), ^{208}Pb (500 µs), ^{232}Th (500 µs), ^{235}U (500 µs), ^{238}U (250 µs).
Mass cycle time (s)	0.1668	0.1418
IC Dead time (ns)	16.7	10.0
Total signal acquisition time per spot	40 s	
Total baseline acquisition time per spot	40 s	
Laser-mode parameters:		
Laser energy:	3–5 mJ	
Energy density:	3 and 5 J cm^{-2}	4–5 J cm^{-2}
Spot size:	95 µm	85–135 µm
Repetition rate:	5 and 8 Hz	5 Hz
Cell & carrier He gas:	*ca* 0.65 L min^{-1}	0.25–0.40 L min^{-1}
Make-up Ar gas:	*ca* 0.34 L min^{-1}	0.25–0.38 L min^{-1}
Accessory N_2 gas:	*ca* 3.0 mL min^{-1}	5.5–6.0 mL min^{-1}
Ni sampler cone:	"Dry" plasma type, 0.9 mm orifice	
Ni skimmer cone:	"Dry" plasma type, 0.7 mm orifice	
Total U sensitivity	Session 1: ~8.7× 10^4 cps µg/g^{-1} Session 2: ~1.1 × 10^5 cps µg/g^{-1} Session 3: ~5.4 × 10^4 cps µg/g^{-1} (NIST614, 95 µm spot)	All sessions: ~2.8× 10^4 cps µg/g^{-1} (NIST612, 85 µm spot)

References

Amelin, Y., Beljaev, A., Larin, A., Neymark, L.A., and Stepanov, K., 1991, Salmi batholith and Pitkäranta ore field in Soviet Karelia, *in* Haapala, I., Rämö, O.T., and Salonsaari, P.T. eds., Rapakivi Granites and Related Rocks, Espoo, Geological Survey of Finland. https://tupa.gtk.fi/julkaisu/opas/op_033.pdf

Amelin, Y. V, Larin, A.M., and Tucker, R.D., 1997, Chronology of multiphase emplacement of the Salmi rapakivi granite-anorthosite complex, Baltic Shield: Implications for magmatic evolution: Contributions to Mineralogy and Petrology, v. 127, p. 353–368, doi:10.1007/s004100050285.

Baker, J., Peate, D., Waight, T., and Meyzen, C., 2004, Pb isotopic analysis of standards and samples using a 207Pb-204Pb double spike and thallium to correct for mass bias with a double-focusing MC-ICP-MS: Chemical Geology, v. 211, p. 275–303, doi:10.1016/j.chemgeo.2004.06.030.

Blevin, P.L., and Norman, M.D., 2010a, Cassiterite the zircon of mineral systems? A scoping study, *in* Australian Earth Sciences Convention, Canberra, 4-8 July 2010, Geological Survey of New South Wales; NSW Department of Industry and Investment.

Blevin, P.L., and Norman, M.D., 2010b, Cassiterite the zircon of mineral systems? A scoping study, *in* Australian Earth Sciences Convention, Canberra, 4-8 July 2010, Geological Survey of New South Wales; NSW Department of Industry and Investment.

Brown, R.E., and Stroud, W.J., 1997, Inverelll: 250 000 Metallogenic Map SH/56-5:Metallogenic Study and Mineral Deposit Data Sheets.:

Cao, H.-W., Zhang, Y.-H., Pei, Q.-M., Zhang, R.-Q., Tang, L., Lin, B., and Cai, G.-J., 2017, U–Pb dating of zircon and cassiterite from the Early Cretaceous Jiaojiguan iron-tin polymetallic deposit, implications for magmatism and metallogeny of the Tengchong area, western Yunnan, China: International Geology Review, v. 59, doi:10.1080/00206814.2016.1220842.

Carr, P.A., Norman, M.D., and Bennett, V.C., 2017, Assessment of crystallographic orientation effects on secondary ion mass spectrometry (SIMS) analysis of cassiterite: Chemical Geology, v. 467, doi:10.1016/j.chemgeo.2017.08.003.

Carr, P.A., Zink, S., Bennett, V.C., Norman, M.D., Amelin, Y., and Blevin, P.L., 2020, A new method for U–Pb geochronology of cassiterite by ID-TIMS applied to the Mole Granite polymetallic system, eastern Australia: Chemical Geology, v. 539, doi:10.1016/j.chemgeo.2020.119539.

Cheng, Y., Spandler, C., Kemp, A., Mao, J., Rusk, B., Hu, Y., and Blake, K., 2019, Controls on cassiterite (SnO 2) crystallization: Evidence from cathodoluminescence, trace-element chemistry, and geochronology at the Gejiu Tin District: American Mineralogist, v. 104, p. 118–129, doi:10.2138/am-2019-6466.

Chengyou, F., Dequan, Z., Zailin, Z., and Song, W., 2012, Chronology of the Tungsten Deposits in Southern Jiangxi Province, and Episodes and Zonation of the Regional W-Sn Mineralization - Evidence from High-precision Zircon U–Pb, Molybdenite Re-Os and Muscovite Ar-Ar Ages: Acta Geologica Sinica - English Edition, v. 86, doi:10.1111/j.1755-6724.2012.00685.x.

Chew, D.M., Petrus, J.A., and Kamber, B.S., 2014, U–Pb LA–ICPMS dating using accessory mineral standards with variable common Pb: Chemical Geology, v. 363, doi:10.1016/j.chemgeo.2013.11.006.

Deng, X.-H., Chen, Y.-J., Bagas, L., Zhou, H.-Y., Zheng, Z., Yue, S.-W., Chen, H.-J., Li, H.-M., Tu, J.-R., and Cui, Y.-R., 2018, Cassiterite U–Pb geochronology of the Kekekaerde W-Sn deposit in the Baiganhu ore field, East Kunlun Orogen, NW China: Timing and tectonic setting of mineralization: Ore Geology Reviews, v. 100, doi:10.1016/j.oregeorev.2017.02.018.

Denholm, J.L., Stepanov, A.S., Meffre, S., Bottrill, R.S., and Thompson, J.M., 2021, The Geochronology of Tasmanian Tin Deposits Using LA-ICP-MS U–Pb Cassiterite Dating: Economic Geology, doi:10.5382/econgeo.4837.

Fei, G. et al., 2020, Petrogenesis of the Lijiagou spodumene pegmatites in Songpan-Garze Fold Belt, West Sichuan, China: Evidence from geochemistry, zircon, cassiterite and coltan U–Pb geochronology and Hf isotopic compositions: Lithos, v. 364–365, doi:10.1016/j.lithos.2020.105555.

Fietzke, J., and Frische, M., 2016, Experimental evaluation of elemental behavior during LA-ICP-MS: influences of plasma conditions and limits of plasma robustness: Journal of Analytical Atomic Spectrometry, v. 31, p. 234–244, doi:10.1039/C5JA00253B.

Gemmrich, L., Torró, L., Melgarejo, J.C., Laurent, O., Vallance, J., Chelle-Michou, C., and Sempere, T.P.A., 2021, Trace element composition and U–Pb ages of cassiterite from the Bolivian tin belt: Mineralium Deposita 2021 56:8, v. 56, p. 1491–1520, doi:10.1007/S00126-020-01030-3.

Guillong, M., Kuhn, H.R., and Günther, D., 2003, Application of a particle separation device to reduce inductively coupled plasma-enhanced elemental fractionation in laser ablation-inductively coupled plasma-mass spectrometry, *in* Spectrochimica Acta - Part B Atomic Spectroscopy, v. 58, p. 211–220, doi:10.1016/S0584-8547(02)00257-4.

Gulson, B.L., and Jones, M.T., 1992, Cassiterite: potential for direct dating of mineral deposits and a precise age for the

Bushveld Complex granites: Geology, v. 20, p. 355–358, doi:10.1130/0091-7613(1992)020<0355:CPFDDO>2.3.CO;2.

Guo, J., Zhang, R., Li, C., Sun, W., Hu, Y., Kang, D., and Wu, J., 2018, Genesis of the Gaosong Sn–Cu deposit, Gejiu district, SW China: Constraints from in situ LA-ICP-MS cassiterite U–Pb dating and trace element fingerprinting: Ore Geology Reviews, v. 92, doi:10.1016/j.oregeorev.2017.11.033.

Hiess, J., Condon, D.J., Mclean, N., Noble, S.R., 2012, 238U/235U systematics in terrestrial uranium-bearing minerals. Science, 2012, vol. 335, no 6076, p. 1610-1614, doi:10.1126/science.1215507

Horstwood, M.S.A. et al., 2016, Community-Derived Standards for LA-ICP-MS U-(Th-)Pb Geochronology – Uncertainty Propagation, Age Interpretation and Data Reporting: Geostandards and Geoanalytical Research, v. 40, p. 311–332, doi:10.1111/j.1751-908X.2016.00379.x.

Jackson, S.E., Pearson, N.J., Griffin, W.L., and Belousova, E.A., 2004, The application of laser ablation-inductively coupled plasma-mass spectrometry to in situ U–Pb zircon geochronology: Chemical Geology, v. 211, p. 47–69, doi:10.1016/j.chemgeo.2004.06.017.

Jingwen, M., Xiaofeng, L., Wen, C., Xiaoming, L., and Shaoliu, W., 2010, Geological Characteristics of the Furong Tin Orefield, Hunan, 40Ar-39Ar Dating of Tin Ores and Related Granite and Its Geodynamic Significance for Rock and Ore Formation: Acta Geologica Sinica - English Edition, v. 78, p. 481–491, doi:10.1111/j.1755-6724.2004.tb00158.x.

Jochum, K.P. et al., 2011, Determination of Reference Values for NIST SRM 610-617 Glasses Following ISO Guidelines: Geostandards and Geoanalytical Research, v. 35, doi:10.1111/j.1751-908X.2011.00120.x.

Kendall-Langley, L.A., Kemp, A.I.S., Grigson, J.L., and Hammerli, J., 2020, U–Pb and reconnaissance Lu-Hf isotope analysis of cassiterite and columbite group minerals from Archean Li-Cs-Ta type pegmatites of Western Australia: Lithos, v. 352–353, p. 105231, doi:10.1016/j.lithos.2019.105231.

Kroslakova, I., and Günther, D., 2007a, Elemental fractionation in laser ablation-inductively coupled plasma-mass spectrometry: Evidence for mass load induced matrix effects in the ICP during ablation of a silicate glass: Journal of Analytical Atomic Spectrometry, v. 22, p. 51–62, doi:10.1039/b606522h.

Kroslakova, I., and Günther, D., 2007b, Elemental fractionation in laser ablation-inductively coupled plasma-mass spectrometry: Evidence for mass load induced matrix effects in the ICP during ablation of a silicate glass: Journal of Analytical Atomic Spectrometry, v. 22, p. 51–62, doi:10.1039/b606522h.

Kuhn, B.K., Birbaum, K., Luo, Y., and Günther, D., 2010a, Fundamental studies on the ablation behaviour of Pb/U in NIST 610 and zircon 91500 using laser ablation inductively coupled plasma mass spectrometry with respect to geochronology: Journal of Analytical Atomic Spectrometry, v. 25, p. 21–27, doi:10.1039/b917261k.

Kuhn, B.K., Birbaum, K., Luo, Y., and Günther, D., 2010b, Fundamental studies on the ablation behaviour of Pb/U in NIST 610 and zircon 91500 using laser ablation inductively coupled plasma mass spectrometry with respect to geochronology: J. Anal. At. Spectrom., v. 25, p. 21–27, doi:10.1039/B917261K.

Larin, A., Neymark, L., and Amelin, Y., 1991, Relation of the mineralization in the Pitkäranta ore district to the Salmi batholith: Geological Survey of Finaldn, v. 33, p. 42–45.

Lehmann, B., 2020, Formation of tin ore deposits: A reassessment: Lithos, doi:10.1016/j.lithos.2020.105756.

Li, C., Zhang, R., Ding, X., Ling, M., Fan, W., and Sun, W., 2016, Dating cassiterite using laser ablation ICP-MS: Ore Geology Reviews, v. 72, doi:10.1016/j.oregeorev.2015.07.016.

Liu, P., Mao, J., Lehmann, B., Peng, L., Zhang, R., Wang, F., Lu, G., and Jiang, C., 2021, Cassiterite U–Pb dating of the lower Cretaceous Yanbei tin porphyry district in the Mikengshan volcanic basin, SE China: Ore Geology Reviews, v. 134, p. 104151, doi:10.1016/J.OREGEOREV.2021.104151.

Liu, C., Wang, R.C., Wu, F.Y., Xie, L., Liu, X.C., Li, X.K., Yang, L., and Li, X.J., 2020a, Spodumene pegmatites from the Pusila pluton in the higher Himalaya, South Tibet: Lithium mineralization in a highly fractionated leucogranite batholith: Lithos, v. 358–359, p. 105421, doi:10.1016/J.LITHOS.2020.105421.

Liu, C., Wang, R.C., Wu, F.Y., Xie, L., Liu, X.C., Li, X.K., Yang, L., and Li, X.J., 2020b, Spodumene pegmatites from the Pusila pluton in the higher Himalaya, South Tibet: Lithium mineralization in a highly fractionated leucogranite batholith: Lithos, v. 358–359, p. 105421, doi:10.1016/J.LITHOS.2020.105421.

Ludwig, K.R., 2008, Isoplot version 4.15: a geochronological toolkit for microsoft Excel: Berkeley Geochronology Center, Special Publication,.

Marcoux, É., Barré, B., Pichavant, M., and Poujol, M., 2021, Âge et genèse de la coupole granitique à métaux rares (Sn, Li, Nb-Ta, W) de Montebras (Creuse, Massif central français) (E. Marcoux, Ed.): BSGF - Earth Sciences Bulletin, v. 192, p. 16, doi:10.1051/bsgf/2020042.

Nambaje, C., Williams, I.S., and Sajeev, K., 2021, SHRIMP U–Pb dating of cassiterite: Insights into the timing of Rwandan tin mineralisation and associated tectonic processes: Ore Geology Reviews, v. 135, p. 104185, doi:10.1016/j.oregeorev.2021.104185.

Neymark, L.A., Amelin, V.Y., Larin, A.M., 1994, Pb-Nd-Sr isotopic and geochemical constraints on the origin of the 1.54–1.56 Ga Salmi rapakivi granite—Anorthosite batholith (Karelia, Russia). Miner. Pet. 50, 173–193, doi:10.1007/bf01160146.

Neymark, L.A., Holm-Denoma, C.S., Larin, A.M., Moscati, R.J., and Plotkina, Y. V., 2021, LA-ICPMS U–Pb dating reveals cassiterite inheritance in the Yazov granite, Eastern Siberia: Implications for tin mineralization: Mineralium Deposita, doi:10.1007/s00126-020-01038-9.

Neymark, L.A., Holm-Denoma, C.S., and Moscati, R.J., 2018, In situ LA-ICPMS U–Pb dating of cassiterite without a known-age matrix-matched reference material: Examples from worldwide tin deposits spanning the Proterozoic to the Tertiary: Chemical Geology, v. 483, doi:10.1016/j.chemgeo.2018.03.008.

Oberthür, T., Melcher, F., Goldmann, S., Wotruba, H., Gerdes, A., Dijkstra, A., and Dale, C.W., 2016, Mineralogy and mineral chemistry of detrital heavy minerals from the Rhine River in Germany as evidence to their provenance, sedimentary and depositional history: focus on platinum-group minerals and remarks on cassiterite, columbite-group minerals and ur: International Journal of Earth Sciences, v. 105, p. 637–657, doi:10.1007/s00531-015-1181-3.

P.L., B., and Norman, M.D., 2010, Cassiterite the zircon of mineral systems? A scoping study, *in* Australian Earth Sciences Convention, Canberra, 4-8 July 2010, Geological Survey of New South Wales; NSW Department of Industry and Investment, https://search.geoscience.nsw.gov.au/product/1249.

Paton, C., Hellstrom, J., Paul, B., Woodhead, J., and Hergt, J., 2011, Iolite: Freeware for the visualisation and processing of mass spectrometric data: Journal of Analytical Atomic Spectrometry, v. 26, p. 2508–2518, doi:10.1039/c1ja10172b.

Paton, C., Woodhead, J.D., Hellstrom, J.C., Hergt, J.M., Greig, A., and Maas, R., 2010, Improved laser ablation U–Pb zircon geochronology through robust downhole fractionation correction: Geochemistry, Geophysics, Geosystems, v. 11, doi:10.1029/2009GC002618.

Peng, J.T., Hu, R.Z., Bi, X.W., Dai, T.M., Li, Z.L., Shuang, Y., Yuan, S.D., and Liu, S.R., 2007, 40Ar/39Ar isotopic dating of tin mineralization in Furong deposit of Hunan Province and its geological significance: Mineral Deposits, v. 26, p. 237–248.

Pietruszka, A.J., and Neymark, L.A., 2017, Evaluation of laser ablation double-focusing SC-ICPMS for “common” lead isotopic measurements in silicate glasses and minerals: Journal of Analytical Atomic Spectrometry, v. 32, doi:10.1039/C7JA00005G.

Rizvanova, N.G., and Kuznetsov, A.B., 2020, A New Approach to ID-TIMS U–Pb Dating of Cassiterite by the Example of the Pitkäranta Tin Deposit: Doklady Earth Sciences, v. 491, doi:10.1134/S1028334X20030150.

Schaltegger, U., Pettke, T., Audétat, A., Reusser, E., and Heinrich, C.A., 2005, Magmatic-to-hydrothermal crystallization in the W–Sn mineralized Mole Granite (NSW, Australia): Chemical Geology, v. 220, doi:10.1016/j.chemgeo.2005.02.018.

Stacey, J.S.S., and Kramers, J.D.D., 1975, Approximation of terrestrial lead isotope evolution by a two-stage model: Earth and Planetary Science Letters, v. 26, p. 207–221, doi:10.1016/0012-821X(75)90088-6.

Tapster, S., and Bright, J.W.G., 2020, High-precision ID-TIMS cassiterite U–Pb systematics using a low-contamination hydrothermal decomposition: implications for LA-ICP-MS and ore deposit geochronology: Geochronology, v. 2, doi:10.5194/gchron-2-425-2020.

Vermeesch, P., 2018, IsoplotR: A free and open toolbox for geochronology: Geoscience Frontiers, v. 9, p. 1479–1493, doi:10.1016/j.gsf.2018.04.001.

Wiedenbeck, M., Allé, P., Corfu, F., Griffin, W.L., Meier, M., Oberli, F., Quadt, A. Von, Roddick, J.C., and Spiegel, W., 1995, Three natural zircon standards for U-Th-Pb, Lu-Hf, trace element and REE analyses: Geostandards and Geoanalytical Research, v. 19, doi:10.1111/j.1751-908X.1995.tb00147.x.

Williams, I.S., 1998, U-Th-Pb Geochronology by Ion Microprobe, *in* McKibben, M.A., Shanks III, W.C., and Ridley, W.I. eds., Applications of Microanalytical Techniques to Understanding Mineralizing Processes, v. 7, p. 1–35.

Yang, J.-H., Zhou, M.-F., Hu, R.-Z., Zhong, H., Williams-Jones, A.E., Liu, L., Zhang, X.-C., Fu, Y.-Z., and Mao, W., 2020, Granite-Related Tin Metallogenic Events and Key Controlling Factors in Peninsular Malaysia, Southeast Asia: New Insights from Cassiterite U–Pb Dating and Zircon Geochemistry: Economic Geology, v. 115, doi:10.5382/econgeo.4736.

Yang, M., Romer, R.L., Yang, Y.H., Wu, S.T., Wang, H., Tu, J.R., Zhou, H.Y., Xie, L.W., Huang, C., Xu, L., Yang, J.H., and Wu, F.Y., 2022, U-Pb isotopic dating of cassiterite: Development of reference materials and in situ applications by LA-SF-ICP-MS. Chemical Geology, 593, 120754, doi: https://doi.org/10.1016/j.chemgeo.2022.120754

Yu, Z., Norman, M.D., and Robinson, P., 2003, Major and Trace Element Analysis of Silicate Rocks by XRF and Laser Ablation ICP-MS Using Lithium Borate Fused Glasses: Matrix Effects, Instrument Response and Results for International Reference Materials: Geostandards and Geoanalytical Research, v. 27, p. 67–89, doi:10.1111/j.1751-908X.2003.tb00713.x.

Yuan, S., Peng, J., Hao, S., Li, H., Geng, J., and Zhang, D., 2011, In situ LA-MC-ICP-MS and ID-TIMS U–Pb geochronology

of cassiterite in the giant Furong tin deposit, Hunan Province, South China: New constraints on the timing of tin–polymetallic mineralization: Ore Geology Reviews, v. 43, doi:10.1016/j.oregeorev.2011.08.002.

Zhang, R., Lehmann, B., Seltmann, R., Sun, W., and Li, C., 2017, Cassiterite U–Pb geochronology constrains magmatic-hydrothermal evolution in complex evolved granite systems: The classic Erzgebirge tin province (Saxony and Bohemia): Geology, v. 45, p. 1095–1098, doi:10.1130/G39634.1.

Zhang, S., Zhang, R., Lu, J., Ma, D., Ding, T., Gao, S., and Zhang, Q., 2019, Neoproterozoic tin mineralization in South China: geology and cassiterite U–Pb age of the Baotan tin deposit in northern Guangxi: Mineralium Deposita, v. 54, doi:10.1007/s00126-019-00862-y.